Micromechanical modelling of cohesive thermoelastic cracking in orthotropic polycrystalline materials

G. Geraci[a,*], M.H. Aliabadi[a]

[a] *Department of Aeronautics, Imperial College London, London, SW7 2AZ, UK*

Abstract

In this paper a new micromechanical formulation is proposed for modelling thermoelastic intergranular and transgranular damage and microcracking evolution in brittle polycrystalline materials. Polycrystalline microstructures are created through a Voronoi tessellation algorithm. Each crystal has an elastic orthotropic behaviour. Damage evolution along (inter- or trans- granular) interfaces is modelled using thermo-mechanical cohesive laws and, upon failure, non-linear frictional contact analysis is introduced to model separation, stick or slip. Numerical simulations are presented either to demonstrate the validity and study the physical implications of the proposed thermoelastic formulation, in comparison with other numerical methods as well as experimental observations and literature results.

Keywords: thermo-elasticity, transgranular, intergranular, orthotropic polycrystalline, cohesive microfracture, boundary element method

1. Introduction

It is well established that damage and microcracking of polycrystalline materials depend on a synergism of factors [1, 2]: single grain's elastic properties, material anisotropy, grain's morphology, grain's size distribution in the aggregate and mismatches between adjacent crystals are a few examples. However a pivotal role in the development of damage and the residual life of these materials is played by the effect of temperature. The thermal effect can be considered either due to long exposure of the component to high temperature or cooling down from fabrication to room temperature or for other thermal treatments such as quenching. As it has been mentioned in [1], the material crystallographic structure affects the initiation of micro-cracking, but also temperature excursion, grain size, boundary vs grain critical energies and the so called thermal-expansion-induced microcracking play important roles: (i) non-cubic single-phase polycrystalline aggregates experience differential expansion due to thermal expansion anisotropy (TEA) in single phase materials; (ii) differential thermal expansion

*Corresponding author.

Email addresses: giorgio.geraci13@imperial.ac.uk (G. Geraci), m.h.aliabadi@imperial.ac.uk (M.H. Aliabadi)

due to mismatch of thermal expansion/contraction, even in isotropic but multi-phase polycrystalline materials, might generate residual stresses between adjacent grains and damage onset could occur.

In polycrystalline materials the modes of fracture are classified as follows: brittle intergranular and transgranular cracking, ductile failure and at high temperature creep has to be taken into account. It is worth noting however that Blendell and Coble in [3] have measured stresses development due to thermal expansion anisotropy in Al_2O_3 and showed that the microstructure does not experience any stress relaxation until very high temperature, close to the annealing. Thus in this work the effect of creep has not been considered since the thermal loading has been applied within the range of temperatures that guarantees no stress relaxation. Moreover still from the experimental findings in [3], the authors have extrapolated the *stress-free* temperature, from which it is possible to approximate analytically the maximum local stress due to differential thermal expansion.

Experimental methods may be used for such investigations, even though sometimes they might be expensive and time consuming due to specific required techniques. Experimental results on grain size dependence and thermal expansion anisotropy were presented by Rice et al. in [4, 5] as well as spontaneous cracking in [6]. Experiments and simulations were conducted by Yousef et al. [7] where residual stresses due to cooling from stress free status has been investigated. Thermal expansion anisotropy has been studied also in [8] where the effect of microcracking due to local thermal expansion mismatch has a substantial influence on the damage evolution in the polycrystalline aggregates.

A popular and powerful approach to investigate these mechanisms is the use of *computational micromechanic* models. Finite Element Method has been widely used thanks to the availability of commercial software. Grains' interfaces have been modelled as cohesive surfaces to study intergranular damage. The most popular cohesive failure models have been proposed by Camacho and Ortiz, who studied impact damage and propagation of multiple cracks in 2D [9], and the potential based laws by Tvergaard [10] and Xu and Needleman [11]. An extensive review of cohesive traction-separation laws for fracture has been done by Park and Paulino in [12]. Competition between inter- and trans-granular damage has been investigated by many authors, and examples are: Sukumar et al. [13], Qian and Li [14] and Lin et al. [15]. Espinosa and Zavattieri [16, 17] have studied the dynamic fragmentation of ceramics using a cohesive finite element formulation and the role of residual stresses as well as thermal induced microcracking have been investigated.

However when studying thermo-elastic problems, interfaces or cracks may act as barriers for the heat propagation [18], so in the framework of cohesive damage evolution thermo-mechanical cohesive relationships have been developed. William et al. [19] examined the degradation of interfaces in heterogeneous materials due to thermal and mechanical damage; other examples of thermo-mechanical cohesive zone models are the works by Sapora and Paggi [20], Wu and Wriggers [21] and Özdemir et al. [22], where finite element models have been developed in order to describe coupled thermoelastic debonding, temperature and humidity jump across a cohesive crack and the concept of *thermal damage* has been introduced.

Although FEM is widely utilised, in recent years *Boundary Element Method* (BEM) has also gained much popularity [23]; especially when polycrystalline microstructures are studied, BEM allows to discretize and model only the grain boundaries, thus reducing substantially the size of the problem.Moreover the field unknowns are directly the displacements and surface tractions, thus

allowing a straightforward implementation of cohesive laws between the cohesive surfaces. Application of boundary element formulation to intergranular fracture processes in polycrystalline materials is due to Sfantos and Aliabadi [24]. Benedetti and Aliabadi [2] have presented a three-dimensional grain-boundary micromechanical model for intergranular fracture and more recently Benedetti et al. investigated the integranular stress corrosion cracking [25]. *Dual Boundary Element Method* (DBEM) formulation to deal with coplanar surfaces (cracks) embedded within the same domain is due to Portela, Aliabadi and Rooke [26, 27]; application of DBEM to anisotropic linear elastic fracture mechanics (LEFM) and crack growth in orhtotropic laminates is due to Sollero and Aliabadi [28, 29]. More recently Geraci and Aliabadi [1] have presented a cohesive formulation for intergranular and transgranular damage propagation with particular attention to the factors influencing their interaction and hence the mode of fracture in polycrystalline materials. The extension of DBEM to thermoelastic problems is due to Prasad and Aliabadi [30, 31] who dealt with steady-state and transient thermo-mechanical analysis.

In this paper a cohesive thermoelastic boundary element formulation is presented for modelling intergranular and transgranular damage propagation in orthotropic polycrystalline aggregates, under the effect of thermo-mechanical loading, for the first time.

Each grain is modelled as a single crystal with general orthotropic mechanical behaviour and generic material orientation. Grain boundary interfaces as well as cracks within the grains are modelled using cohesive law which allows for nucleation and propagation of cracks under mixed mode conditions. As the generic interface/crack completely deteriorates within its cohesive regime, a non-linear frictional contact analysis is used in order to simulate sliding or sticking contact of free surfaces. The concept of a cohesive model has been extended to the heat conduction across the generic interface, where the heat flux has been considered dependent on the level of damage of the interface. In this way the presence of damage or fracture acts as a barrier for the heat conduction. Furthermore the effect of temperature on the elastic properties has been neglected in the present formulation and average coefficients of thermal expansion have been considered within the temperature range considered [32, 33]

2. Thermo-mechanical cohesive model

In [1] the details of the traction-separation laws used in this model have been presented extensively, thus here only the main conclusions will be summarized. When the work of decohesion due to the opening until failure of a cohesive surface along a generic angle ϕ is evaluated, the normal and tangential contributions can be separated. As the ratio between these two is evaluated, G_{II}/G_I is obtained, and when a potential cohesive law is used, this parameter is assumed implicitly equal to one, causing the damage propagation to be path-independent. In the present work however, this hypothesis has been released so that the cohesive parameters are related through the following relationship:

$$\alpha = \beta^2 \frac{\delta u_n^{crit}}{\delta u_t^{crit}} \frac{G_{II}}{G_I} \tag{1}$$

where the ratio G_{II}/G_I can now be assigned arbitrarily. δu_t^{crit} and δu_n^{crit} are respectively the critical tangential and normal opening displacement of the generic cohesive interface. The traction-separation laws take the form:

$$\begin{cases} t_n = T_{max}\dfrac{1-d}{d}\dfrac{\delta u_n}{\delta u_n^{crit}} \\ t_t = \alpha T_{max}\dfrac{1-d}{d}\dfrac{\delta u_t}{\delta u_t^{crit}} \end{cases} \tag{2}$$

where d represents the *damage status* (monotonically increasing) of a cohesive surface, being $d = 0$ for pristine surfaces and $d = 1$ for completely failed ones.

$$d = \sqrt{\left(\frac{\delta u_n}{\delta u_n^{crit}}\right)^2 + \beta^2\left(\frac{\delta u_t}{\delta u_t^{crit}}\right)^2} \tag{3}$$

δu_n and δu_t are respectively the current normal and tangential displacement jumps of the interface.

The concept of thermal damage, intended as a "reduction in the effective conductivity", has been introduced in this model following [22]. $k^{eff}(d) = (1-d)k^I$ is an effective conductivity and k^I is the interface conductivity which can be calculated using the analogy between thermal and electrical resistance concepts. The heat flux through a plane wall can be expressed as:

$$q = \frac{\Delta\theta}{R_{tot}} \tag{4}$$

where $\Delta\theta$ is the temperature difference and R_{tot} the total *thermal resistance*, that results from a series of N different layers with thicknesses L_i and conductivities k_i:

$$R_{tot} = \sum_{i=1}^{N}\frac{L_i}{k_i} \tag{5}$$

When the above concept is applied to the interface between two grains A and B (or to a transgranular interface), where δu is the opening displacement between the two surfaces of the interface, it is plausible to consider the interface itself as a "multilayer wall" with thickness δu_n and conductivity dependent on the conductivities of the materials of each grain: one portion belongs to grain A and the other to grain B, each one having thickness $\delta u_n/2$, as sketched in Figure 1. Using Eq. (5) one gets:

$$R_{tot} = \frac{\delta u_n/2}{k_A} + \frac{\delta u_n/2}{k_B} = \frac{k_A + k_B}{k_A k_B}\frac{\delta u_n}{2} = \frac{\delta u_n}{k^I} \tag{6}$$

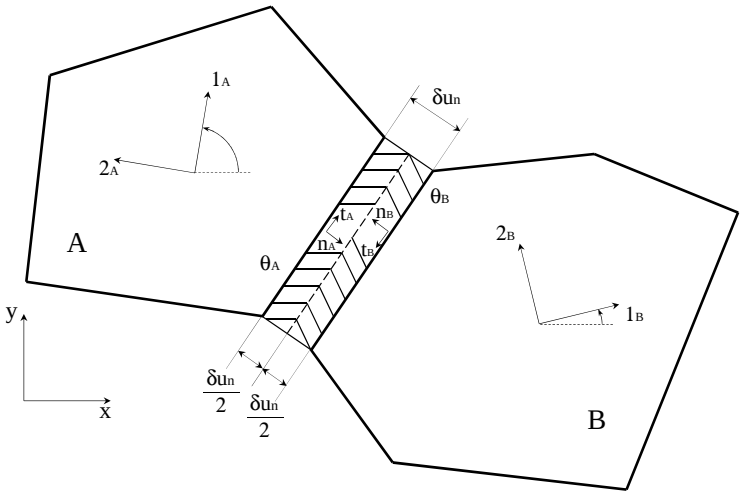


Figure 1: Grains' reference systems and modelling of interface

However it is worth noting that in the most generic case the conductivity k should be considered as a second order tensor; so in local coordinates where t is the tangential direction and n the normal direction to the interface, the conductivity matrix can be written for general orthotropy ($k_{12} = k_{21} = 0$) as:

$$\mathbf{k}^{t-n} = \begin{bmatrix} k_{tt} & k_{tn} \\ k_{tn} & k_{nn} \end{bmatrix} = \begin{bmatrix} -\tilde{n}_y & \tilde{n}_x \\ \tilde{n}_x & \tilde{n}_y \end{bmatrix} \begin{bmatrix} k_{11} & 0 \\ 0 & k_{22} \end{bmatrix} \begin{bmatrix} -\tilde{n}_y & \tilde{n}_x \\ \tilde{n}_x & \tilde{n}_y \end{bmatrix} = \begin{bmatrix} k_{11}\tilde{n}_y^2 + k_{22}\tilde{n}_x^2 & k_{22}\tilde{n}_x\tilde{n}_y - k_{11}\tilde{n}_x\tilde{n}_y \\ sym & k_{11}\tilde{n}_x^2 + k_{22}\tilde{n}_y^2 \end{bmatrix} \tag{7}$$

where subscripts 1 and 2 denote the directions of material orientation and $\tilde{n}_x$ and $\tilde{n}_y$ are the components of the normal unit vector in the local system. However the uncoupling between tangential and normal directions is not guaranteed in the generic local coordinates of the interface: it is evident from Eq. (7) that $k_{tn} = k_{nt} \neq 0$ and hence general anisotropy must be considered.

It is interesting to highlight that in this case the classical definition of flux, i.e. that it is normal to the isothermal surface passing through the spatial position considered, does not apply. This is easy to verify from the previous equations, because when an isothermal surface is considered $\partial\theta/\partial t = 0$, and as long as $k_{nt} \neq 0$, both the component of q are different from zero and hence q is not perpendicular to the isothermal.

Recalling Eq. (4), (6) and (7), then the components of flux at a generic cohesive interface can be written as:

$$\begin{bmatrix} q_t^I \\ q_n^I \end{bmatrix} = - \begin{bmatrix} k_{tt}^I & k_{tn}^I \\ k_{tn}^I & k_{nn}^I \end{bmatrix} \begin{bmatrix} \dfrac{\Delta\theta}{\delta u_t} \\ \dfrac{\Delta\theta}{\delta u_n} \end{bmatrix} \tag{8}$$

where

$$k_{ij}^{I} = 2\frac{k_{ij}^{A}k_{ij}^{B}}{k_{ij}^{A}+k_{ij}^{B}} \qquad \{i,j=t,n\} \tag{9}$$

being A and B either two materials with different properties or two portions of the same material.

Thus the thermal cohesive law, which relates the temperature gradients to the normal flux component, can be expressed as:

$$q_n(d) = -(1-d)\left(\frac{k_{tn}^{I}}{\delta u_t}+\frac{k_{nn}^{I}}{\delta u_n}\right)\Delta\theta \tag{10}$$

It is worth noting that the flux in Eq. (10) is equivalent to the orthotropic flux expressed as:

$$q = -\left(k_{11}\frac{\partial\theta}{\partial x_1}n_1 + k_{22}\frac{\partial\theta}{\partial x_2}n_2\right) \tag{11}$$

In fact the flux in Eq. (11) is obtained by rotating the components of flux from material to local coordinates and by taking only the component normal to the surface under examination. Equation (10) is expressed in function of direct variables of the current problem so in this work it is more convenient to rotate the conductivity matrix and deal with tangential and normal components.

3. Anisotropic steady-state thermoelasticity

3.1. Overview

Here the equations for steady-state, linear, elastic, anisotropic and homogeneous body occupying a domain V enclosed by a boundary S are shown, and then simplifications for orthotropy condition will be applied. The most general thermoelastic problems are governed by the Navier's equation (equation of motion) and the Euler's equation (heat conduction equation).

$$\begin{cases} S_{ijkl}u_{k,lj} - \gamma_{ij}\Delta\theta_{,j} + b_i = 0 \\ k_{ij}\theta_{,ij} = 0 \end{cases} \tag{12}$$

where $\mathbf{S}$ is the stiffness tensor, $\mathbf{u}$ is the displacement, $\mathbf{b}$ is the body force, θ is the temperature and $\gamma_{ij} = S_{ijkl}\alpha_{kl}$, being α_{kl} the coefficients of thermal expansion. The notation $(\cdot)_{,i}$ stands for differentiation with respect to the i^{th} spatial coordinate and Einstein notation applies. Moreover the conductivity coefficients k_{ij} are related through thermodynamics principles and Onsager's reciprocity [34, 35]:

$$k_{11} > 0 \ ; \ k_{22} > 0 \ ; \ k_{11}k_{22} - k_{12}^2 > 0 \ ; \ k_{12} = k_{21} \tag{13}$$

Constitutive relationship when temperature changes $\Delta\theta$ are considered can be expressed by the well known Duhamel-Neumann relation:

$$\sigma_{ij} = S_{ijkl}\ \varepsilon_{kl} - \gamma_{ij}\Delta\theta \tag{14}$$

It is worth noting that in this work plane strain condition for 2D model has been applied. In the thermoelastic case the condition defining plane strain is $\varepsilon_{zz}^{tot} = \varepsilon_{zz}^{mech} + \varepsilon_{zz}^{\theta} = 0$, and it is easy to notice that if the temperature variation is different from zero there will be a mechanical strain in z direction $\varepsilon_{zz}^{mech} = -\varepsilon_{zz}^{\theta} \neq 0$. The generic direct stress component for orthotropic plane strain thermoelasticity can be expressed as follows:

$$\sigma_{ii} = S_{ij}\varepsilon_{jj}^{tot} - (S_{il}\alpha_{ll})\Delta\theta \qquad j = 1, 2\ ;\ i, l = 1, 2, 3 \tag{15}$$

where Voight notation has been used. Hence also the components S_{13} and S_{23} have to be considered explicitly, even with plane strain condition, if thermo-mechanical behaviour has to be investigated. In case of isotropic thermoelasticity the additional term would be expressed by:

$$S_{il}\alpha\Delta\theta = \frac{E}{1-2\nu}\alpha\Delta\theta \qquad i, l = 1, 2, 3 \tag{16}$$

being E the Young's modulus and ν the Poisson's ratio. In order to obtain the solution to Eq. (12) for the determination of temperature, fluxes, displacements and tractions in polycrystalline aggregates, in this work the boundary element method has been used. Due to the nature of the domain under examination, a *multi-region* and *dual-boundary element* formulations need to be considered. Since the formulation dealing with the transition between intergranular and transgranular damage has been extensively covered in [1], here the final set of equations is reported and more attention is focused on the thermoelastic aspects. For the sake of clarity let us consider a generic polycrystalline aggregate as shown in Figure 2 where the surfaces of each grain $H = 1 \dots N_g$ can be classified as: non-contact (S_{nc}^H) resulting from the intersection between grains and the outer domain's boundary, contact (S_c^H) which are the interfaces between adjacent grains, and transgranular coplanar surfaces ($S_{cr^{+,-}}^H$). The following relationships apply [1]:

$$S_*^H = S_{nc}^H \cup S_c^H \quad ; \quad S^H = S_*^H \cup (S_{cr^+}^H \cup S_{cr^-}^H) \tag{17}$$

Following Prasad and Aliabadi [30], the boundary integral equations involved in the solution of the problem are the Displacement, Traction, Temperature and Flux equations.

In this work the problem is formulated in terms of opening displacements of the transgranular interfaces (δu_{cr}) and temperature jumps ($\delta\theta_{cr}$); this choice is helpful since a cohesive thermo-mechanical approach has been used, so that tractions and opening displacements are related as well as fluxes and temperature jumps. With this premises, when the mechanical and the thermal problems are solved together for numerical convenience (even though it is an uncoupled problem), the system of equations to be solved is composed by:

- Displacement equation for collocation on S_*^H

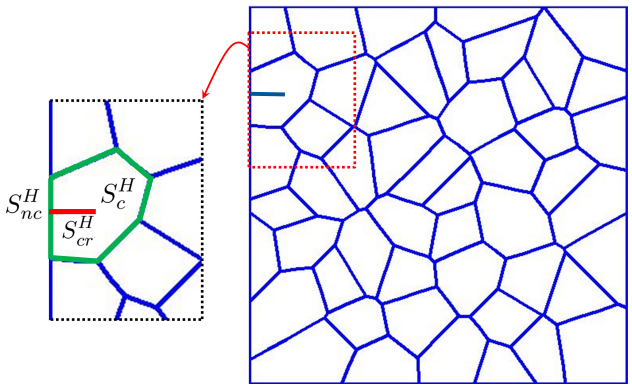


Figure 2: Surfaces in polycrystalline aggregate (intergranular and transgranular)

- Traction equation for collocation on S_{cr}^H
- Temperature equation for collocation on S_*^H
- Temperature equation for collocation on S_{cr}^H
- Flux equation for collocation on S_{cr}^H

It is worth noting that although the dual BEM has been used, an additional temperature equation for collocation on the transgranular elements needs to be introduced. For the pure thermal problem then, the only flux equation would be sufficient for collocation on transgranular elements, but the actual temperature of the crack would be still unknown. However the traction equation cannot be expressed only in terms of the temperature difference across the crack, but both temperatures are required or one temperature and the difference. In other words the mechanical solutions to two thermo-elastic problems having the same crack's temperature jump but different actual temperatures (e.g. $\theta_1^{cr^+} = 5°C$, $\theta_1^{cr^-} = 10°C$ and $\theta_2^{cr^+} = 200°C$, $\theta_2^{cr^-} = 205°C$) are different, as intuitively understandable. If instead the thermal problem was solved separately, an additional temperature equation would be required anyway in post-processing to retrieve the temperature of one of the crack's surfaces.

3.2. Domain mapping

It is worth noting at this point that the last two terms in the Navier's equation (Eq. (12)) can be considered as an effective body force $b_i' = b_i - \gamma_{ij}\Delta\theta_{,j}$. The presence of this term however generates an additional volume integral in the aforementioned boundary integral equations. In case of isotropic thermoelasticity the governing equation of conduction is the well known Laplace's equation and then the transformation of the volume integral into a surface integral (known as ETM, i.e.

exact transformation method) is obtained using the Galerkin vector and the condition $\theta_{,ii} = 0$, as explained in [36]; however in non-isotropic media the first step of the ETM is to map the domain into a coordinate system where the temperature field can be governed by a canonical Laplace's equation. This procedure has been developed by Shiah and Tan [37]. In their work the details of the domain mapping have been extensively presented, so here only the main results, and the adaptation to orthotropic materials will be shown. The method of characteristics has been used to obtain two consecutive coordinate transformations with which the final mapped domain is related to the orthotropic ($k_{11} \neq k_{22}$ and $k_{12} = k_{21} = 0$) through the following:

$$\begin{cases} x_{\underline{1}} &= \sqrt{\frac{k_{22}}{k_{11}}} x_1 \\ x_{\underline{2}} &= x_2 \end{cases} \tag{18}$$

With the transformation in Eq. (18) the following ralationship is then true:

$$\theta_{,\underline{11}} + \theta_{,\underline{22}} = 0 \tag{19}$$

where the underlined values are intended in the mapped domain. The following relationships also apply [38].

$$\begin{cases} \theta_{,\underline{1}} = \theta_{,1} \sqrt{\frac{k_{11}}{k_{22}}} \\ \theta_{,\underline{2}} = \theta_{,2} \end{cases} \quad \Rightarrow J = \sqrt{\frac{k_{22}}{k_{11}}} \tag{20}$$

$$\begin{cases} \gamma_{\underline{11}} = \gamma_{11} \\ \gamma_{\underline{22}} = \gamma_{22} \sqrt{\frac{k_{11}}{k_{22}}} \end{cases} \tag{21}$$

$$\begin{cases} n_{\underline{1}} = n_1 \frac{l}{\hat{l}} \\ n_{\underline{2}} = n_2 \frac{l}{\hat{l}} \sqrt{\frac{k_{22}}{k_{11}}} \end{cases} \qquad \begin{cases} l = \sqrt{\Delta x_1^2 + \Delta x_2^2} \\ \hat{l} = \sqrt{\frac{k_{22}}{k_{11}} \Delta x_1^2 + \Delta x_2^2} \end{cases} \tag{22}$$

where J is the Jacobian of the transformation, and l and $\hat{l}$ the generic lengths respectively in the original and in the mapped domain. This mapping has been introduced for the sake of completeness and coherently with the complex analysis of the anisotropic formulation.

3.3. Boundary Integral Equations

The boundary integral equations are written below, where fundamental solutions related to opposite coplanar surfaces have been simplified already and the kind of surfaces introduced in Eq. (17) have been considered explicitly; the temperature change will be indicated only with θ for the sake of brevity, and interface boundary conditions on cracks have been applied as:

$$\begin{cases} \delta\tilde{\mathbf{u}}(\mathbf{x}_{cr}) = \tilde{\mathbf{u}}(\mathbf{x}^+) + \tilde{\mathbf{u}}(\mathbf{x}^-) \\ \tilde{\mathbf{t}}(\mathbf{x}_{cr}) = \tilde{\mathbf{t}}(\mathbf{x}^+) = \tilde{\mathbf{t}}(\mathbf{x}^-) \end{cases} ; \quad \begin{cases} \delta\theta(\mathbf{x}_{cr}) = \theta(\mathbf{x}^+) - \theta(\mathbf{x}^-) \\ q(\mathbf{x}_{cr}) = q(\mathbf{x}^+) = -q(\mathbf{x}^-) \end{cases} \tag{23}$$

Displacement Equation

$$
\begin{aligned}
C_{ij}^{H}(\mathbf{x}')\tilde{u}_{j}^{H}(\mathbf{x}') = & \int_{\tilde{S}_{*}^{H}} \tilde{U}_{ij}^{H}(\mathbf{x}',\mathbf{x})\tilde{t}_{j}^{H}(\mathbf{x})d\tilde{S}_{*}^{H} - \fint_{\tilde{S}_{*}^{H}} \tilde{T}_{ij}^{H}(\mathbf{x}',\mathbf{x})\tilde{u}_{j}^{H}(\mathbf{x})d\tilde{S}_{*}^{H} + \\
& - \int_{\tilde{S}_{cr}^{H}} \tilde{T}_{ij}^{H}(\mathbf{x}',\mathbf{x}_{cr})\delta\tilde{u}_{j}^{H}(\mathbf{x}_{cr})d\tilde{S}_{cr}^{H} + \int_{\hat{\tilde{S}}_{*}^{H}} P_{\underline{i}}^{H}(\mathbf{x}',\mathbf{x})\theta^{H}(\mathbf{x})d\hat{\tilde{S}}_{*}^{H} + \\
& + \int_{\hat{\tilde{S}}_{cr}^{H}} P_{\underline{i}}^{H}(\mathbf{x}',\mathbf{x}_{cr})\delta\theta^{H}(\mathbf{x}_{cr})d\hat{\tilde{S}}_{cr}^{H} - \int_{\tilde{S}_{*}^{H}} Q_{\underline{i}}^{H}(\mathbf{x}',\mathbf{x})q^{H}(\mathbf{x})d\tilde{S}_{*}^{H}
\end{aligned}
\tag{24}
$$

Traction Equation

$$
\begin{aligned}
\tilde{t}_{j}^{H}(\mathbf{x}'_{cr}) = & \tilde{n}_{i}(\mathbf{x}^{+})\fint_{\tilde{S}_{*}^{H}} \tilde{D}_{kij}^{H}(\mathbf{x}^{+},\mathbf{x})\tilde{t}_{k}^{H}(\mathbf{x})d\tilde{S}_{*}^{H} - \tilde{n}_{i}(\mathbf{x}^{+})\fint_{\tilde{S}_{*}^{H}} \tilde{S}_{kij}^{H}(\mathbf{x}^{+},\mathbf{x})\tilde{u}_{k}^{H}(\mathbf{x})d\tilde{S}_{*}^{H} + \\
& - \tilde{n}_{i}(\mathbf{x}^{+})\fint_{\tilde{S}_{cr}^{H}} \tilde{S}_{kij}^{H}(\mathbf{x}^{+},\mathbf{x}_{cr})\delta\tilde{u}_{k}^{H}(\mathbf{x}_{cr})d\tilde{S}_{cr}^{H} + \tilde{n}_{i}(\mathbf{x}^{+})\fint_{\hat{\tilde{S}}_{*}^{H}} P_{\underline{ij}}^{H}(\mathbf{x}^{+},\mathbf{x})\theta^{H}(\mathbf{x})d\hat{\tilde{S}}_{*}^{H} + \\
& + \tilde{n}_{i}(\mathbf{x}^{+})\fint_{\hat{\tilde{S}}_{cr}^{H}} P_{\underline{ij}}^{H}(\mathbf{x}^{+},\mathbf{x}_{cr})\delta\theta^{H}(\mathbf{x}_{cr})d\hat{\tilde{S}}_{cr}^{H} - \tilde{n}_{i}(\mathbf{x}^{+})\fint_{\tilde{S}_{*}^{H}} Q_{\underline{ij}}^{H}(\mathbf{x}^{+},\mathbf{x})q^{H}(\mathbf{x})d\tilde{S}_{*}^{H} + \\
& - \tilde{n}_{i}(\mathbf{x}^{+})2S_{j3}\alpha_{33}\delta_{ij}\theta^{H}(\mathbf{x}_{cr}) + \tilde{n}_{i}(\mathbf{x}^{+})S_{j3}\alpha_{33}\delta_{ij}\delta\theta^{H}(\mathbf{x}_{cr})
\end{aligned}
\tag{25}
$$

In Eq. (25) the term $S_{j3}\alpha_{33}$ explicitly accounts for the additional stress component due to the thermal effect; the other components $S_{j1}\alpha_{11}$ and $S_{j2}\alpha_{22}$ are implicitly taken into account since from the derivation of the displacement equation the mechanical strains in direction 1 and 2 are already obtained. The fundamental solutions D_{kij}, S_{kij}, $P_{\underline{ij}}$ and $Q_{\underline{ij}}$ are obtained from the differentiation with respect to the collocation point of U_{ij}, T_{ij}, $P_{\underline{i}}$ and $Q_{\underline{i}}$ respectively, and subsequent application of the constitutive law.

Temperature Equations

$$
\begin{aligned}
C^{H}(\mathbf{x}')\theta^{H}(\mathbf{x}') = & \int_{\tilde{S}_{*}^{H}} {q^{*}}^{H}(\mathbf{x}',\mathbf{x})\theta(\mathbf{x})d\tilde{S}_{*}^{H} - \int_{\tilde{S}_{*}^{H}} {\theta^{*}}^{H}(\mathbf{x}',\mathbf{x})q(\mathbf{x})d\tilde{S}_{*}^{H} + \\
& + \int_{\tilde{S}_{cr}^{H}} {q^{*}}^{H}(\mathbf{x}',\mathbf{x}_{cr})\delta\theta(\mathbf{x}_{cr})d\tilde{S}_{cr}^{H}
\end{aligned}
\tag{26}
$$

$$
\begin{aligned}
\theta^{H}(\mathbf{x}'_{cr}) - \frac{1}{2}\delta\theta^{H}(\mathbf{x}'_{cr}) = & \int_{\tilde{S}_{*}^{H}} {q^{*}}^{H}(\mathbf{x}^{+},\mathbf{x})\theta(\mathbf{x})d\tilde{S}_{*}^{H} - \int_{\tilde{S}_{*}^{H}} {\theta^{*}}^{H}(\mathbf{x}^{+},\mathbf{x})q(\mathbf{x})d\tilde{S}_{*}^{H} + \\
& + \int_{\tilde{S}_{cr}^{H}} {q^{*}}^{H}(\mathbf{x}^{+},\mathbf{x}_{cr})\delta\theta(\mathbf{x}_{cr})d\tilde{S}_{cr}^{H}
\end{aligned}
\tag{27}
$$

where θ^* is the fundamental solution to the governing equation [39]:

$$k_{11}\frac{\partial^2\theta}{\partial x_1^2}+k_{22}\frac{\partial^2\theta}{\partial x_2^2}=0 \tag{28}$$

$$\theta^*=-\frac{1}{2\pi\sqrt{k_1k_2}}\log(r_{orth}) \tag{29}$$

being r_{orth}

$$r_{orth}(\mathbf{x}',\mathbf{x})=\sqrt{\frac{1}{k_1}(x_1-x_1')^2+\frac{1}{k_2}(x_2-x_2')^2} \tag{30}$$

and q^* is obtained by substituting Eq. (29) into Eq. (11).

Flux Equation

$$\begin{aligned}q^H(\mathbf{x}'_{cr}) =&\tilde{n}_i(\mathbf{x}^+)\oint_{\tilde{S}_*^H}\theta_i^{**}(\mathbf{x}^+,\mathbf{x})q^H(\mathbf{x})d\tilde{S}_*^H-\tilde{n}_i(\mathbf{x}^+)\oint_{\tilde{S}_*^H}q_i^{**}(\mathbf{x}^+,\mathbf{x})\theta^H(\mathbf{x})d\tilde{S}_*^H+\\&-\tilde{n}_i(\mathbf{x}^+)\oint_{\tilde{S}_{cr}^H}q_i^{**}(\mathbf{x}^+,\mathbf{x}_{cr})\delta\theta^H(\mathbf{x}_{cr})d\tilde{S}_{cr}^H\end{aligned} \tag{31}$$

The flux equation for a boundary point is obtained from derivation of the temperature equation with respect to the collocation point and application of Eq. (11). The same applies also for the fundamental solutions θ^{**} and q^{**} [36].

The set of equations (24-27) and (31) can be written in matrix form for each grain $H=1,\ldots,N_g$ as follows:

$$\begin{bmatrix}\tilde{\mathbf{H}}^d & \tilde{\mathbf{H}}^d_{cr} & \mathbf{H}^d_\theta & \mathbf{0} & \mathbf{H}^d_{\theta_{cr}}\\ \tilde{\mathbf{H}}^t & \tilde{\mathbf{H}}^t_{cr} & \mathbf{H}^t_\theta & 2\mathbf{I}c & \mathbf{I}c+\mathbf{H}^t_{\theta_{cr}}\\ \mathbf{0} & \mathbf{0} & \mathbf{H}^\theta_\theta & \mathbf{0} & \mathbf{H}^\theta_{\theta_{cr}}\\ \mathbf{0} & \mathbf{0} & \mathbf{H}^{\theta_{cr}}_\theta & \mathbf{I} & \mathbf{H}^{\theta_{cr}}_{\theta_{cr}}\\ \mathbf{0} & \mathbf{0} & \mathbf{H}^q_\theta & \mathbf{0} & \mathbf{H}^q_{\theta_{cr}}\end{bmatrix}\begin{Bmatrix}\tilde{\mathbf{u}}\\ \delta\tilde{\mathbf{u}}_{cr}\\ \boldsymbol{\theta}\\ \boldsymbol{\theta}_{cr}\\ \delta\boldsymbol{\theta}_{cr}\end{Bmatrix}=\begin{bmatrix}\tilde{\mathbf{G}}^d & \mathbf{0} & \mathbf{G}^d_\theta & \mathbf{0}\\ \tilde{\mathbf{G}}^t & \mathbf{I} & \mathbf{G}^t_\theta & \mathbf{0}\\ \mathbf{0} & \mathbf{0} & \mathbf{G}^\theta_\theta & \mathbf{0}\\ \mathbf{0} & \mathbf{0} & \mathbf{G}^{\theta_{cr}}_\theta & \mathbf{0}\\ \mathbf{0} & \mathbf{0} & \mathbf{G}^q_\theta & \mathbf{G}^q_{\theta_{cr}}\end{bmatrix}\begin{Bmatrix}\tilde{\mathbf{t}}\\ \delta\tilde{\mathbf{t}}_{cr}\\ \mathbf{q}\\ \mathbf{q}_{cr}\end{Bmatrix} \tag{32}$$

where the superscripts d, t, θ, θ_{cr} and q stand for *displacement*, *traction*, *temperature*, *temperature on crack* and *flux* equation respectively, $c=S_{j3}\alpha_{33}$, as previously seen in the traction equation. $\mathbf{I}$ is an identity sub-matrix and $\mathbf{0}$ a null sub-matrix. $\tilde{\mathbf{u}}$ and $\tilde{\mathbf{t}}$ contain known and unknown values of displacements and tractions respectively on contact and non-contact surfaces, $\delta\tilde{\mathbf{u}}_{cr}$ and $\delta\tilde{\mathbf{t}}_{cr}$ contain unknown values of jump displacements and tractions respectively on the transgranular surfaces. $\boldsymbol{\theta}$ and $\mathbf{q}$ contain known and unknown values of temperatures and fluxes respectively on contact and non-contact surfaces; $\boldsymbol{\theta}_{cr}$, $\mathbf{q}_{cr}$ and $\delta\boldsymbol{\theta}_{cr}$ contain respectively unknown values of temperature, fluxes

and temperature difference across the transgranular surface. The symbol $\tilde{(\cdot)}$ refers to a field in the tangential and normal reference system of the local surface (see Appendix D for more details).

After applying the boundary condition and re-arranging the matrices, the system can be expressed as in Eq. (33). This final matrix has been written for two generic n^{th} and m^{th} grains sharing an interface; this has been done to highlight how the system of matrix is rearranged and how interface boundary conditions are applied to the system. The field variables have been divided into known and unknown vectors: $\tilde{\mathbf{x}}$ and $\mathbf{x}_\theta$ contain mixed terms respectively of unknown displacement or tractions and temperatures or fluxes on the outer boundary (S_{nc}); $\tilde{\mathbf{y}}$ and $\mathbf{y}_\theta$ contain known values of the aforementioned fields, applied through the boundary conditions. Sub-matrices $\mathbf{A}$ and $\mathbf{B}$ contain mixed component of $\mathbf{H}$ and $\mathbf{G}$ and sub-matrices $\mathbf{\Phi}$ contain the cohesive laws relating $\delta\mathbf{u}$ to $\mathbf{t}$ and $\delta\theta$ to q. Moreover the right hand side has been divided into two vectors, one containing only mechanical variables ($\mathbf{F}^m$) and the other only thermal variables ($\mathbf{F}^\theta$); this helps in applying different loading factors to the mechanical or the thermal boundary conditions during the incremental loading procedure.

$$
\left[\begin{array}{ccccccccccccc}
\tilde{\mathbf{A}}^{d^n} & \mathbf{A}_\theta^{d^n} & \tilde{\mathbf{H}}_I^{d^n} & \mathbf{0} & \tilde{\mathbf{H}}_{cr}^{d^n} & \text{-}\tilde{\mathbf{G}}_I^{d^n} & \mathbf{0} & \mathbf{H}_{\theta I}^{d^n} & \mathbf{0} & \mathbf{0} & \mathbf{H}_{\theta_{cr}}^{d^n} & \text{-}\mathbf{G}_{\theta I}^{d^n} & \mathbf{0} \\
\tilde{\mathbf{A}}^{t^n} & \mathbf{A}_\theta^{t^n} & \tilde{\mathbf{H}}_I^{t^n} & \mathbf{0} & \tilde{\mathbf{H}}_{cr}^{t^n} & \text{-}\tilde{\mathbf{G}}_I^{t^n} & \mathbf{I} & \mathbf{H}_{\theta I}^{t^n} & 2c\mathbf{I} & \mathbf{0} & c\mathbf{I}+\mathbf{H}_{\theta_{cr}}^{t^n} & \text{-}\mathbf{G}_{\theta I}^{t^n} & \mathbf{0} \\
\mathbf{0} & \mathbf{A}^{\theta^n} & \mathbf{0} & \mathbf{0} & \mathbf{0} & \mathbf{0} & \mathbf{0} & \mathbf{H}_{\theta I}^{\theta^n} & \mathbf{0} & \mathbf{0} & \mathbf{H}_{\theta_{cr}}^{\theta^n} & \text{-}\mathbf{G}_{\theta I}^{\theta^n} & \mathbf{0} \\
\mathbf{0} & \mathbf{A}^{\theta_{cr}^n} & \mathbf{0} & \mathbf{0} & \mathbf{0} & \mathbf{0} & \mathbf{0} & \mathbf{H}_{\theta I}^{\theta_{cr}^n} & \mathbf{I} & \mathbf{0} & \mathbf{H}_{\theta_{cr}}^{\theta_{cr}^n} & \text{-}\mathbf{G}_{\theta I}^{\theta_{cr}^n} & \mathbf{0} \\
\mathbf{0} & \mathbf{A}^{q^n} & \mathbf{0} & \mathbf{0} & \mathbf{0} & \mathbf{0} & \mathbf{0} & \mathbf{H}_{\theta I}^{q^n} & \mathbf{0} & \mathbf{0} & \mathbf{H}_{\theta_{cr}}^{q^n} & \text{-}\mathbf{G}_{\theta I}^{q^n} & \text{-}\mathbf{G}_{\theta_{cr}}^{q^n} \\
\hline
\tilde{\mathbf{A}}^{d^m} & \mathbf{A}_\theta^{d^m} & \text{-}\tilde{\mathbf{H}}_I^{d^m} & \tilde{\mathbf{H}}_I^{d^m} & \tilde{\mathbf{H}}_{cr}^{d^m} & \text{-}\tilde{\mathbf{G}}_I^{d^m} & \mathbf{0} & \mathbf{H}_{\theta I}^{d^m} & \mathbf{0} & \text{-}\mathbf{H}_{\theta I}^{d^m} & \mathbf{H}_{\theta_{cr}}^{d^m} & \text{-}\mathbf{G}_{\theta I}^{d^m} & \mathbf{0} \\
\tilde{\mathbf{A}}^{t^m} & \mathbf{A}_\theta^{t^m} & \text{-}\tilde{\mathbf{H}}_I^{t^m} & \tilde{\mathbf{H}}_I^{t^m} & \tilde{\mathbf{H}}_{cr}^{t^m} & \text{-}\tilde{\mathbf{G}}_I^{t^m} & \mathbf{I} & \mathbf{H}_{\theta I}^{t^m} & 2c\mathbf{I} & \text{-}\mathbf{H}_{\theta I}^{t^m} & c\mathbf{I}+\mathbf{H}_{\theta_{cr}}^{t^m} & \text{-}\mathbf{G}_{\theta I}^{t^m} & \mathbf{0} \\
\mathbf{0} & \mathbf{A}^{\theta^m} & \mathbf{0} & \mathbf{0} & \mathbf{0} & \mathbf{0} & \mathbf{0} & \mathbf{H}_{\theta I}^{\theta^m} & \mathbf{0} & \text{-}\mathbf{H}_{\theta I}^{\theta^m} & \mathbf{H}_{\theta_{cr}}^{\theta^m} & \text{-}\mathbf{G}_{\theta I}^{\theta^m} & \mathbf{0} \\
\mathbf{0} & \mathbf{A}^{\theta_{cr}^m} & \mathbf{0} & \mathbf{0} & \mathbf{0} & \mathbf{0} & \mathbf{0} & \mathbf{H}_{\theta I}^{\theta_{cr}^m} & \mathbf{I} & \text{-}\mathbf{H}_{\theta I}^{\theta_{cr}^m} & \mathbf{H}_{\theta_{cr}}^{\theta_{cr}^m} & \text{-}\mathbf{G}_{\theta I}^{\theta_{cr}^m} & \mathbf{0} \\
\mathbf{0} & \mathbf{A}^{q^m} & \mathbf{0} & \mathbf{0} & \mathbf{0} & \mathbf{0} & \mathbf{0} & \mathbf{H}_{\theta I}^{q^m} & \mathbf{0} & \text{-}\mathbf{H}_{\theta I}^{q^m} & \mathbf{H}_{\theta_{cr}}^{q^m} & \text{-}\mathbf{G}_{\theta I}^{q^m} & \text{-}\mathbf{G}_{\theta_{cr}}^{q^m} \\
\hline
\mathbf{0} & \mathbf{0} & \mathbf{0} & \mathbf{\Phi}_I & \mathbf{0} & \mathbf{I} & \mathbf{0} & \mathbf{0} & \mathbf{0} & \mathbf{0} & \mathbf{0} & \mathbf{0} & \mathbf{0} \\
\mathbf{0} & \mathbf{0} & \mathbf{0} & \mathbf{0} & \mathbf{\Phi}_{cr} & \mathbf{0} & \mathbf{I} & \mathbf{0} & \mathbf{0} & \mathbf{0} & \mathbf{0} & \mathbf{0} & \mathbf{0} \\
\mathbf{0} & \mathbf{0} & \mathbf{0} & \mathbf{0} & \mathbf{0} & \mathbf{0} & \mathbf{0} & \mathbf{0} & \mathbf{0} & \mathbf{\Phi}_I^\theta & \mathbf{0} & \mathbf{I} & \mathbf{0} \\
\mathbf{0} & \mathbf{0} & \mathbf{0} & \mathbf{0} & \mathbf{0} & \mathbf{0} & \mathbf{0} & \mathbf{0} & \mathbf{0} & \mathbf{0} & \mathbf{\Phi}_{cr}^\theta & \mathbf{0} & \mathbf{I}
\end{array}\right]
\left\{\begin{array}{c}
\tilde{\mathbf{x}} \\ \mathbf{x}_\theta \\ \tilde{\mathbf{u}}^I \\ \delta\tilde{\mathbf{u}}^I \\ \delta\tilde{\mathbf{u}}^{cr} \\ \tilde{\mathbf{t}}^I \\ \tilde{\mathbf{t}}^{cr} \\ \boldsymbol{\theta}_I \\ \boldsymbol{\theta}_{cr} \\ \delta\boldsymbol{\theta}_I \\ \delta\boldsymbol{\theta}_{cr} \\ \mathbf{q}_I \\ \mathbf{q}_{cr}
\end{array}\right\}
=
\left\{\begin{array}{c}
\tilde{\mathbf{B}}^{d^n}\cdot\tilde{\mathbf{y}} \\ \tilde{\mathbf{B}}^{t^n}\cdot\tilde{\mathbf{y}} \\ \mathbf{0} \\ \mathbf{0} \\ \mathbf{0} \\ \hline
\tilde{\mathbf{B}}^{d^m}\cdot\tilde{\mathbf{y}} \\ \tilde{\mathbf{B}}^{t^m}\cdot\tilde{\mathbf{y}} \\ \mathbf{0} \\ \mathbf{0} \\ \mathbf{0} \\ \hline
\mathbf{0} \\ \mathbf{0}
\end{array}\right\}
+
\left\{\begin{array}{c}
\mathbf{B}_\theta^{d^n}\cdot\mathbf{y}_\theta \\ \mathbf{B}_\theta^{t^n}\cdot\mathbf{y}_\theta \\ \mathbf{B}_\theta^{\theta^n}\cdot\mathbf{y}_\theta \\ \mathbf{B}_\theta^{\theta_{cr}^n}\cdot\mathbf{y}_\theta \\ \mathbf{B}_\theta^{q^n}\cdot\mathbf{y}_\theta \\ \hline
\mathbf{B}_\theta^{d^m}\cdot\mathbf{y}_\theta \\ \mathbf{B}_\theta^{t^m}\cdot\mathbf{y}_\theta \\ \mathbf{B}_\theta^{\theta^m}\cdot\mathbf{y}_\theta \\ \mathbf{B}_\theta^{\theta_{cr}^m}\cdot\mathbf{y}_\theta \\ \mathbf{B}_\theta^{q^m}\cdot\mathbf{y}_\theta \\ \hline
\mathbf{0} \\ \mathbf{0}
\end{array}\right\}
\tag{33}
$$

4. Results and examples

In this section the numerical simulations performed using the proposed formulations are presented. In order to validate the method and the formulation, a few examples have been reproduced and compared to either literature or commercial software results.

It is well known that two of the most studied advanced ceramic materials are *aluminium oxide* (Al_2O_3), also known as alumina, and *silicon carbide* (SiC); some comparisons between the thermomechanical behaviours of these two materials have been done in this work and materials' properties are shown in Table 1 in terms of stiffness matrix (S_{ij}) and thermal expansion (α_{ij}) components [7, 24, 32, 33]. It is worth noting that transverse isotropy has been considered, being 1-2 the isotropic plane; the simulations have been run considering the plane 2-3 coplanar to x-y ($1 \equiv z$), and random planar grains' orientation.

A measure for the anisotropy of materials are A^{el} for elasticity (known as Zener ratio) and A^{α} for thermal expansion:

$$\begin{cases} A^{el} = \dfrac{2S_{44}}{(S_{11} - S_{12})} \\ A^{\alpha} = \dfrac{\alpha_{11}}{\alpha_{22}} - 1 \end{cases} \tag{34}$$

Values of A^{el} and A^{α} for both materials are shown in Table 2.

Before showing the details of the simulations, it is convenient to define some parameters in order to facilitate the interpretation of results and the comparison between different scenarios. An interesting parameter for a first analysis of damage measurement is introduced here, comparable to

Table 1: Materials' properties

Property	**SiC**	**Al_2O_3**
S_{11}	501 GPa	442 GPa
S_{33}	565 GPa	473 GPa
S_{12}	95 GPa	109 GPa
S_{13}	96 GPa	73 GPa
S_{44}	169 GPa	147 GPa
S_{66}	203 GPa	167 GPa
α_{11}	$4.46 \times 10^{-6}/°C$	$9.5 \times 10^{-6}/°C$
α_{22}	$4.06 \times 10^{-6}/°C$	$8.6 \times 10^{-6}/°C$
K_{IC}	3 $MPa\sqrt{m}$	
μ_{frict}	0.2	

Table 2: Elastic and thermal coefficients of anisotropy

Property	**SiC**	**Al_2O_3**
A^{el}	0.832	0.883
A^{α}	0.098	0.105

the number of broken bond defined in Sridar et al. [8]:

$$\rho_c = \sum_{\substack{i=1 \\ \forall i: d(i)>0}}^{N_{int}} \frac{2L_i}{L_{int}} \qquad [0 \leq \rho_c \leq 1] \tag{35}$$

This parameter expresses the cumulative length of damage as a fraction of the total interfaces' length. Thus N_{int} is the number of interfaces (including transgranular ones), $2L_i$ and $d(i)$ are respectively the length and damage level (Eq. (3)) of the i^{th} element, and L_{int} is the total length of the microstructure's interfaces. So the problem here has been studied in terms of cohesive damage instead of broken bonds. However the parameter ρ_c does not provide information on the level of damage and degradation of the microstructure, i.e. on the residual strength of the material. So here an additional parameter to describe the damage process has been chosen: in the framework of multi-scale analysis, since we are dealing with micro-structures, the damage parameter D needs to be introduced. For every loading step the total average stress can be evaluated by means of averaging theorems [40]:

$$\bar{\sigma}_{ij} = \frac{1}{V} \int_S x_i t_j dS \tag{36}$$

This integral can be easily evaluated considering only the outer boundary of the aggregate since all the internal interfaces or possible discontinuities are in equilibrium or traction free. The overall decremental stress is then defined as [41]:

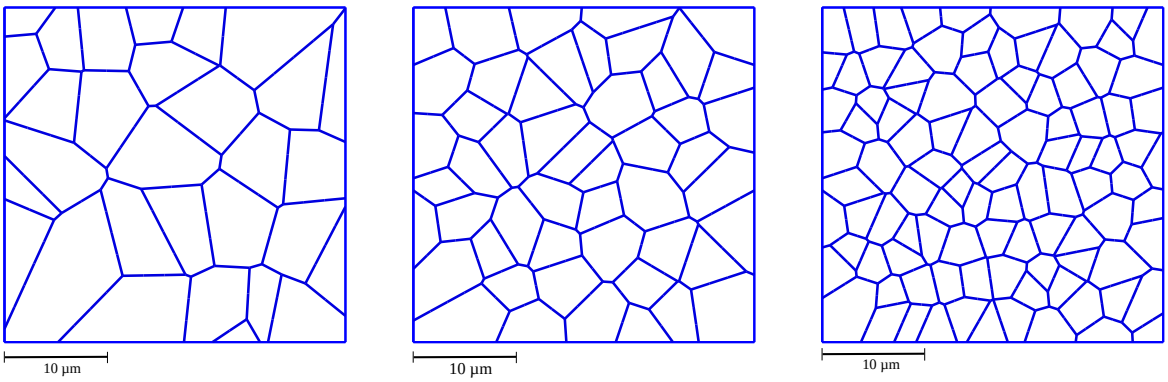
$$\bar{\boldsymbol{\sigma}}^D = \boldsymbol{\sigma}^e - \bar{\boldsymbol{\sigma}}^t \tag{37}$$

where $\boldsymbol{\sigma}^e$ is the elastic stress obtained in absence of any micro-damage and $\bar{\boldsymbol{\sigma}}^t$ is the actual overall stress evaluated using Eq. (36). Hence

$$\sigma_{ij}^D = D_{ij} S_{ijkl} (\varepsilon_{kl}^{tot} - \varepsilon_{kl}^{\theta} \delta_{kl}) = D_{ij} \sigma_{ij}^e \tag{38}$$

Then in virtue of Eq. (37) and (38):

$$\mathbf{D} = 1 - \bar{\boldsymbol{\sigma}}^t [\boldsymbol{\sigma}^e]^{-1} \tag{39}$$



(a) 30 grains, $G = 11.7$. **(b)** 50 grains, $G = 12.5$. **(c)** 100 grains, $G = 13.5$.

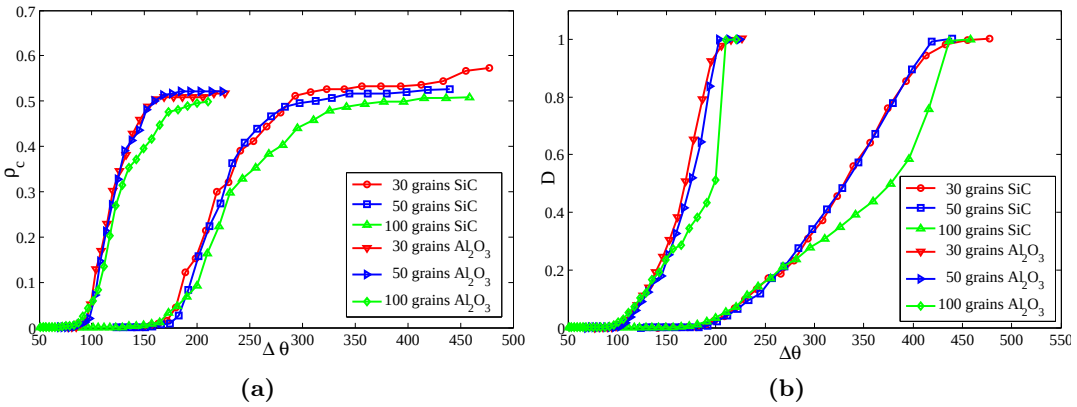
Figure 3: Microstructures with different grain sizes.

From Eq. (39) it is interesting to note that depending on the loading condition and then on the direction of damage propagation (if a preferential direction is present), the overall effect could be an increase of the anisotropy level of the aggregate: if the macro-damage evolves in y direction due to any load along the x axes, the main softening of the microstructure will occur in the x direction and hence the predominant decremental damage component will be D_{11}.

For the sake of completeness, an investigation on the behaviour of the two different materials considered here has been conducted for different grain sizes. Figure 3 shows three of the microstructures on which the simulations have been performed; grain size has been defined according to $ASTM\ E112\text{-}13$: 30 grains with an average grain size $G = 11.7$ ($\bar{A}_{gr} = 37.17\ \mu m^2$, $\bar{d}_{gr} = 6.1\ \mu m$), 50 grains with $G = 12.5$ ($\bar{A}_{gr} = 22.3\ \mu m^2$, $\bar{d}_{gr} = 4.72\ \mu m$) and 100 grains with $G = 13.5$ ($\bar{A}_{gr} = 11.15\ \mu m^2$, $\bar{d}_{gr} = 3.34\ \mu m$); in all the cases the side length of the square microstructure is $l = 33.39 \mu m$. In this first analysis the microstructures have been constrained along the right and left edges and a cooling thermal loading $\Delta\theta$ has been applied uniformly. Figure 4(a) and (b) show respectively the cumulative length of damaged interfaces and the damage (degradation) level at different values of thermal loading. The effect of grain refinement improves the thermal resistance of the aggregate and this feature is in common to both the materials; however it is also clear from both the graphs that the SiC microstructures have a much higher thermal resistance than Al_2O_3. In these simulations a ratio between critical energies of boundaries and grains' interior $R = G_{inter}/G_{trans} = 0.7$ has been chosen to simulate weak grain boundaries; this value of R has been shown, from simulations in uni-axial tension [1], the minimum for which intergranular/transgranular transition occurs but without any critical damage development through the grains, for the morphologies under examinations.

4.0.1. Effect of grain size

Next, damage and micro-cracking propagation have been investigated in silicon carbide microstructures that have been rigidly constrained as if held between the grips of a testing machine. When the



(a) **(b)**

Figure 4: (a) Cumulative length of damaged interfaces ρ_c and (b) damage D as a function of the thermal load $\Delta\theta$ for different grain sizes of silicon carbide and alumina.

edges of the aggregates are constrained and a quasi-static thermal load is applied, the mechanical strain is different from zero and equal and opposite to the overall thermal strain ($\varepsilon^{mech} = -\varepsilon^{\theta}$), which consequently causes a net tensile stress that is conceptually very similar to the effect of mechanical loading. This overall stress is superimposed to the local effect of differential thermal expansion; however as it will be shown the net tensile stress is predominant and it is the mechanism driving damage propagation. For the sake of conciseness and since it is believed that phenomenologically here the damage development depends strongly on the interaction between intergranular and transgranular microcracking, in this section only the case of tough grain boundaries has been considered ($R = 1$).

Figure 5 shows the evolution of damage in the three microstructures considered, where the left and right edges have been fully constrained while top and bottom edges have been considered traction free; increasing uniform cooling thermal load ($\Delta\theta < 0$) has been applied across the microstructures. It is interesting to notice that by comparing the three cracking developments, the coarse grain morphologies are more prone to experience transgranular damage than finer ones; this behaviour results in smoother crack paths as the grain size increases, in good agreement with [1].

The cumulative damage length is presented in Figure 6(a). The curves reach a saturation in ρ_c that is attributable to the development of a main crack whose length is comparable to the size of the microstructure, without any other critical damage being spread in the aggregates. Considering the 50 and 100 grains microstructures the curves show a higher percentage of damaged interfaces in the finer aggregate. It is interesting to notice though that between $150°C$ and $200°C$ the relationship between these curves is inverted, i.e. the coarser grains develop more damage than the finer; this behaviour explains what happens at higher temperatures: since the region of stress relief upon damage onset or crack formation scales as a^2 (a being the length of crack), the higher ρ_c at small $\Delta\theta$ for coarse grain size is equivalent to the formation of longer cracks, which hence relieves stresses on a larger surface, preventing in this way the growth of additional damage. In other words, according to [8], $\rho_c \propto 1/\bar{d}_{gr}$.

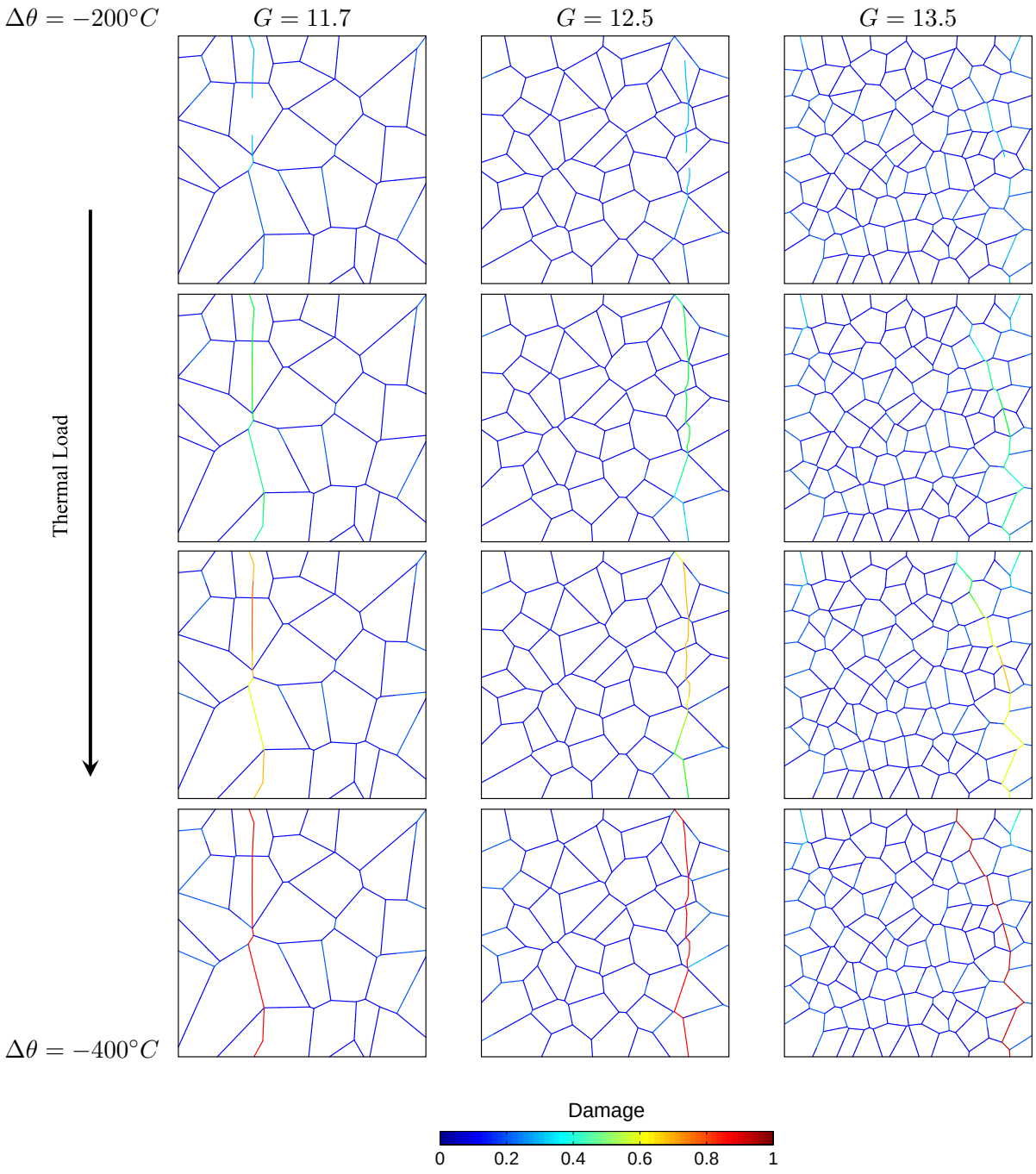
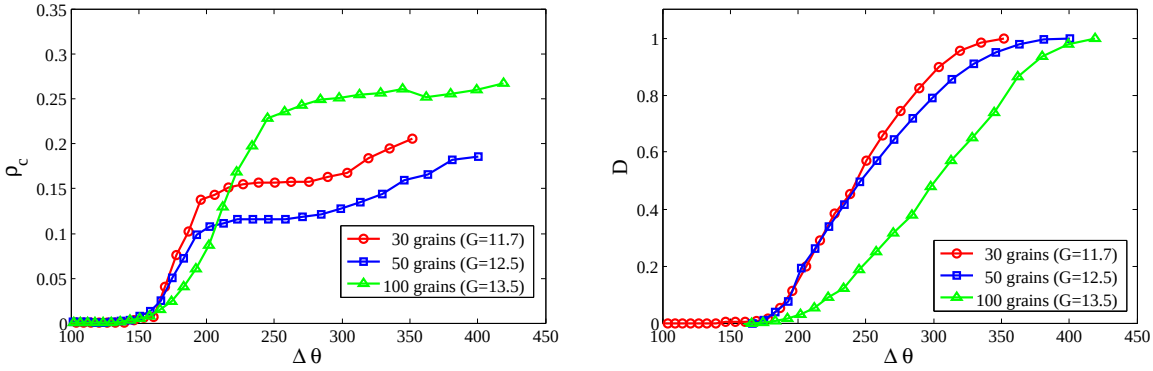


Figure 5: Inter-granular and Trans-granular damage evolution for different sizes of grains G and $R = 1$.



(a) **(b)**

Figure 6: (a) Cumulative length of damaged intergranular and transgranular interfaces ρ_c and (b) damage D as a function of the thermal load $\Delta\theta$ for constrained microstructures and $R = 1$.

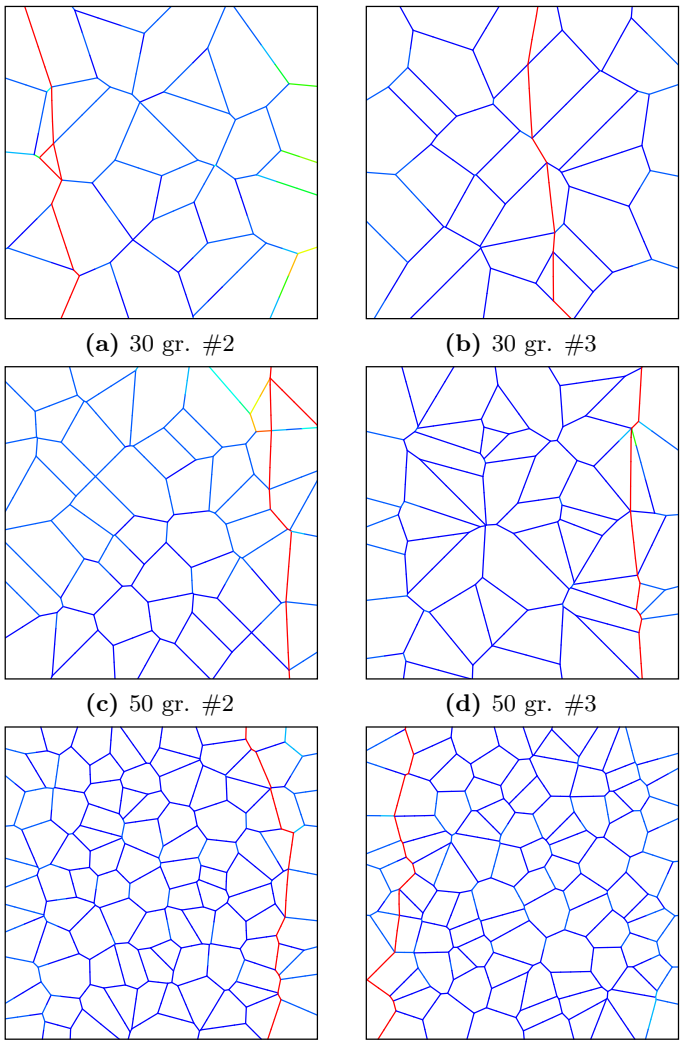
Moreover Figure 6(a) shows that at high $\Delta\theta$ the curve relative to the coarsest aggregate ($G = 11.7$) falls between the other two; hence if the problem was studied considering only the length of damaged interfaces (independently from the level of degradation), those curves would suggest that excessive grain refinement could be detrimental for the microstructure; this behaviour depends of course on the delicate interaction and competition between the inter- and trans- granular modes of fracture, whose balance gives the overall microscopic behaviour of the polycrystalline aggregate.

However it is for this reason that, in the framework of multi-scale applications where the properties at the macroscale are retrieved through the features at the microscale, the degradation parameter D introduced in Eq. (39) has been used here to obtain more information on the residual strength of the three microstructures. From Figure 6(b) it is easy to notice that the degradation of the microstructure is faster as the grain size decreases. This behaviour is in good agreement with the case of mechanical loading where, generally speaking, coarse grain structures show a more brittle behaviour than finer grains.

For the sake of statistical relevance and in order to guarantee that the phenomena captured in the previous examples are not caused by numerical inaccuracy, the above results have been obtained from three different morphologies for each grain size and then averaged. Damage paths in these additional microstructures are shown in Figure 7.

4.1. Spontaneous damage and residual stresses

For the sake of completeness, another application is worth attention. Polycrystalline materials, and ceramics more specifically are known to develop spontaneous damage when subject to thermal loading, even in absence of any external constrain; the physical phenomenon of this behaviour lies in what is called thermal-expansion-induced microcracking and in single-phase, orthotropic (or anisotropic) materials, the cause is the differential thermal expansion between adjacent grains



(a) 30 gr. #2 **(b)** 30 gr. #3

(c) 50 gr. #2 **(d)** 50 gr. #3

(e) 100 gr. #2 **(f)** 100 gr. #3

Figure 7: Final damage patterns in additional morphologies considered.

(TEA)[8]. Hence the two factors that majorly affect this behaviour are the material orientation of each grain and, with reference to Table 2, the level of thermal anisotropy of the material. It is worth noting however that for the materials under consideration in this work, the level of anisotropy is not high, hence in these simulations the extent of micro-damage is very limited and it is more appropriate to analyse the phenomenon by looking at the internal residual stresses due to thermal load and thermal expansion anisotropy. Figure 8 shows a comparison between aluminium oxide and silicon carbide microstructures, that have the same morphology as well as distribution of grains' orientation; a uniform thermal loading, without any external constrain (only rigid motion has been

suppressed) has been applied from the stress-free status to $\Delta\theta = -1200°C$. As it is possible to see each grain develops residual local stresses at the end of the thermal loading. According to [3] the maximum stress between two grains occurs when material axis 1 of the first grain is perpendicular to the boundary and axis 1 of the adjacent grain is parallel to the boundary; hence the following stress can be calculated:

$$\sigma_{max} = \frac{(\alpha_{11} - \alpha_{22})(\theta_{sf} - \theta)}{C_{eff}} \tag{40}$$

where θ_{sf} is the stress-free temperature, θ the current temperature and C_{eff} is the effective material compliance that depends on the actual compliance components, the morphology and the orientation of the grains; an approximation of this value could be $C_{eff} = C_{11} + C_{33}$ for materials having low levels of anisotropy. Moreover the respective legends in Figure 8 show different stress levels for the two materials and this confirms again that SiC has a better thermal resistance than Al_2O_3, as in the example presented in Figure 4 for constrained aggregates. Finally, since only direct components of strain are involved in thermal expansion/contraction, in orthotropic materials (i.e. no coupling like in isotropic) no shear stress would be expected. However due to the polycrystalline structure with generic material orientations for each grain, a general anisotropic behaviour is obtained here, as it is clear from the overall coupling between direct strains and shear stresses that are further increased by the local mismatch between adjacent grains (see the two last plots in Figure 8).

This kind of investigation is important because the presence of residual stresses in the structure, for example after cooling down from production temperatures, can be detrimental for the operational life of the material or the structural component. It is worth noting that if residual tensile stresses can lead to microcraking and reduction of residual life, on the other hand compressive residual stresses could be desirable, depending on the application considered, in order to enhance some properties of interest; this is the case of some thermal treatments.

5. Conclusion

In this paper the effect of thermo-mechanical loading has been studied in polycrystalline microstructures with orthotropic material properties by the newly developed micromechanical BEM. Results have been presented and the features of stress development, damage onset and propagation due to thermal loading have been highlighted. It is clear from the results that the level of anisotropy and the crystallographic orientation of each grain can affect the performance of the aggregate either with or without external constraints. Moreover the effect of grain size has been studied and results are shown to be in good agreement with literature findings as well as analogous to the damage development due to mechanical loading. The cohesive formulation introduced in this paper has given an interesting insight on the damage evolution: depending on the material properties, the constraining and loading condition, not only can the damage propagation be studied in terms of damage length, but the degradation of the microstructure can be retrieved in the framework of multiscale analysis. Bearing in mind that thermal processes are commonly done at the beginning of the operational life of the structural component, all these different behaviours affect its residual life

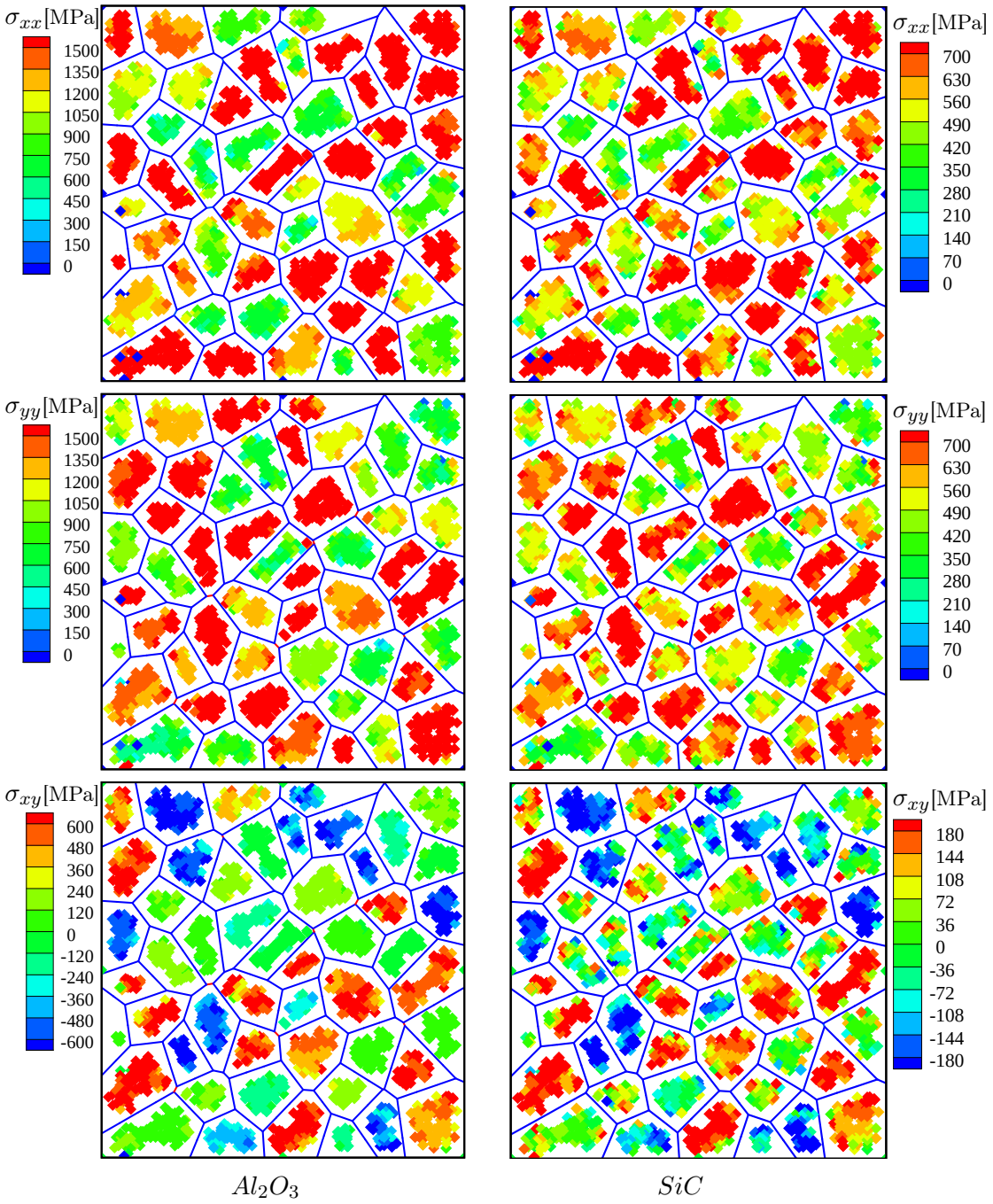


Figure 8: Internal stresses developed due to thermal loading ($\Delta\theta = -1200°C$) and local thermal expansion mismatch in 50 grains Al_2O_3 and SiC microstructures.

and hence understanding the microscopic behaviour of polycrystalline materials become key in order to be able to predict the behaviour of macroscopic components.

A. Material modelling

In this study the grains of the randomly generated microstructures are described by an elastic orthotropic model. The constitutive equations defining the relationship between stresses and strains of each grain are:

$$\varepsilon_{ij} = C_{ijkl}\ \sigma_{kl} \tag{A.1}$$

where C_{ijkl} are the components of the fourth order compliance tensor $\mathbf{C}$. For the sake of conciseness Voight notation will be used in this paper, so that the component of the fourth order tensors will be referred to as follow: $C_{1122} = C_{12}$, $C_{1112} = C_{16}$, $C_{2323} = C_{44}$ and so on with the other component $C_{ij} = C_{ji}$, being $i, j = 1, 2, \ldots, 6$. Since orthotropic or transversally isotropic materials have been considered, some simplifications apply: $C_{14} = C_{15} = C_{16} = 0$, $C_{24} = C_{25} = C_{26} = 0$, $C_{34} = C_{35} = C_{36} = 0$, $C_{45} = C_{46} = C_{56} = 0$. Moreover, in order to be able to consider either plane strain or plane stress conditions in $2D$ problems, the following tensor has been considered:

$$\mathbf{C}' = \begin{bmatrix} C'_{11} & C'_{12} & C'_{16} \\ \ddots & C'_{22} & C'_{26} \\ sym & \ddots & C'_{66} \end{bmatrix} \tag{A.2}$$

where the components of the above matrix are defined in Table A.3 for *plane stress* case or in Table A.4 for *plane strain*.

B. Anisotropy, orthotropy and transversal isotropy considerations

As mentioned before, each grain behaves as fully anisotropic in the global system of coordinate xyz. Thus considering anisotropic elasticity, the complex stress approach needs to be used in order to obtain the fundamental solutions required in the BEM [1]. Let us consider the characteristic equation, whose fulfilment guarantees the existence of a non-trivial solution to the governing differential equation for the Airy stress function:

$$C'_{11}\mu^4 - 2C'_{16}\mu^3 + (2C'_{12} + C'_{66})\mu^2 - 2C'_{26}\mu + C'_{22} = 0 \tag{B.1}$$

Table A.3: 2D and 3D compliance tensor correspondence for *plane stress* condition ($\sigma_z = \tau_{xz} = \tau_{yz}$).

C'_{ij}	$1 \equiv z$	$2 \equiv z$	$3 \equiv z$
C'_{11}	C_{22}	C_{11}	C_{11}
C'_{22}	C_{33}	C_{33}	C_{22}
C'_{12}	C_{23}	C_{13}	C_{12}
C'_{66}	C_{44}	C_{55}	C_{66}

Table A.4: 2D and 3D compliance tensor correspondence for *plane strain* condition ($\varepsilon_z = \gamma_{xz} = \gamma_{yz}$).

$1 \equiv z$	$2 \equiv z$	$3 \equiv z$
$C'_{ij} = C_{kl} - \dfrac{C_{k1} - C_{l1}}{C_{11}}$	$C'_{ij} = C_{kl} - \dfrac{C_{k2} - C_{l2}}{C_{22}}$	$C'_{ij} = C_{kl} - \dfrac{C_{k3} - C_{l3}}{C_{33}}$
$\begin{Bmatrix} i,j \\ k,l \end{Bmatrix} = \begin{Bmatrix} 1,2,6 \\ 2,3,4 \end{Bmatrix}$	$\begin{Bmatrix} i,j \\ k,l \end{Bmatrix} = \begin{Bmatrix} 1,2,6 \\ 1,3,5 \end{Bmatrix}$	$\begin{Bmatrix} i,j \\ k,l \end{Bmatrix} = \begin{Bmatrix} 1,2,6 \\ 1,2,6 \end{Bmatrix}$

The complex roots of Eq. (B.1) are the eigenvalues μ_k; the parameters involved in the evaluation of the anisotropic fundamental solutions, that will be shown in Appendix C are defined as follows:

$$\mathbf{p} = \begin{bmatrix} C'_{11}\mu_1^2 + C'_{12} - C'_{16}\mu_1 & C'_{11}\mu_2^2 + C'_{12} - C'_{16}\mu_2 \\ C'_{12}\mu_1 + C'_{22}/\mu_1 - C'_{26} & C'_{12}\mu_2 + C'_{22}/\mu_2 - C'_{26} \end{bmatrix} \tag{B.2}$$

$$\mathbf{q} = \begin{bmatrix} \mu_1 & \mu_2 \\ -1 & -1 \end{bmatrix} \tag{B.3}$$

The parameters A_{jk} are obtained instead by solving the following system of equations:

$$\begin{bmatrix} 1 & -1 & 1 & -1 \\ \mu_1 & -\bar{\mu}_1 & \mu_2 & -\bar{\mu}_2 \\ p_{11} & -\bar{p}_{11} & p_{12} & -\bar{p}_{12} \\ p_{21} & -\bar{p}_{21} & p_{22} & -\bar{p}_{22} \end{bmatrix} \begin{Bmatrix} A_{j1} \\ \bar{A}_{j1} \\ A_{j2} \\ \bar{A}_{j2} \end{Bmatrix} = \begin{Bmatrix} \delta_{j2}/2\pi i \\ -\delta_{j1}/2\pi i \\ 0 \\ 0 \end{Bmatrix} \tag{B.4}$$

where the notation $\bar{(\cdot)}$ denotes the complex conjugate.

It is easy to show that for orthotropic materials, in which $C'_{16} = C'_{26} = 0$, Eq. (B.1) becomes

$$C'_{11}\mu^4 + (2C'_{12} + C'_{66})\mu^2 + C'_{22} = 0 \tag{B.5}$$

In this case the solutions of the characteristic equation are:

$$\mu_k = \frac{i}{\sqrt{a_k}} \qquad \text{where} \quad k = 1, 2 \quad \text{and} \quad i = \sqrt{-1} \tag{B.6}$$

Matrix $\mathbf{p}$ becomes:

$$\mathbf{p} = \begin{bmatrix} C'_{11}\mu_1^2 + C'_{12} & C'_{11}\mu_2^2 + C'_{12} \\ C'_{12}\mu_1 + C'_{22}/\mu_1 & C'_{12}\mu_2 + C'_{22}/\mu_2 \end{bmatrix} = \begin{bmatrix} A_2 & A_1 \\ \dfrac{1}{\mu_1}(-\dfrac{A_1}{a_1}) & \dfrac{1}{\mu_2}(-\dfrac{A_2}{a_2}) \end{bmatrix} \tag{B.7}$$

and the following relationships apply:

$$\begin{cases} b = 2\pi(a_1 - a_2)C'_{22} \\ a_1 + a_2 = (2C'_{12} + C'_{66})/C'_{22} \\ a_1 a_2 = C'_{11}/C'_{22} \\ A_k = C'_{12} - a_k C'_{22} \\ r_k = \sqrt{(x_1^{\mathbf{x}-\mathbf{x}'})^2 + \dfrac{(x_2^{\mathbf{x}-\mathbf{x}'})^2}{a_k}} \\ \theta_k = Arg\left(x_1^{\mathbf{x}-\mathbf{x}'} + \frac{x_2^{\mathbf{x}-\mathbf{x}'}}{\sqrt{a_k}}\right) \\ M_k = \sqrt{a_k} x_1^{\mathbf{x}-\mathbf{x}'} n_2 - \dfrac{x_2^{\mathbf{x}-\mathbf{x}'} n_1}{\sqrt{a_k}} \\ \mathbf{x}^{\mathbf{x}-\mathbf{x}'} = \mathbf{x} - \mathbf{x}' \end{cases} \quad ; \quad [k = 1, 2] \tag{B.8}$$

This formulation requires that the material parameters a_k must be real and positive, resulting in $2(\sqrt{C'_{11}C'_{22}} - C'_{12})/C'_{66} \leqslant 1$, that is however a requirement satisfied for a large number of engineering materials.

The fundamental solutions presented in the following section are expressed in function of the generic spatial coordinate z_k, which represents the distance between the collocation point $\mathbf{x}'$ and the integration point $\mathbf{x}$:

$$z = (x_1 - x'_1) + \mu(x_2 - x'_2) \tag{B.9}$$

It is worth noting that even though Eq. (B.4) is singular for $\mu_1 = \mu_2$, the pseudo-isotropic case may be derived by considering the characteristic equation Eq. (B.1) in terms of perturbed isotropic material, in which $E_1 = E_2 + \varepsilon$, for ε small.

C. ETM and Fundamental solutions

Let us consider a generic integral boundary displacement equation:

$$\begin{aligned} C_{ij}(\mathbf{x}')u_j(\mathbf{x}') = &\int_S U_{ij}(\mathbf{x}', \mathbf{x})t_j(\mathbf{x})dS - \oint_S T_{ij}(\mathbf{x}', \mathbf{x})u_j(\mathbf{x})dS + \\ &+ \int_V U_{ij}(\mathbf{X}', \mathbf{X})b'_j(\mathbf{X})dV \end{aligned} \tag{C.1}$$

When the term b'_j is written explicitly, the following is obtained

$$\begin{aligned} C_{ij}(\mathbf{x}')u_j(\mathbf{x}') = &\int_S U_{ij}(\mathbf{x}', \mathbf{x})t_j(\mathbf{x})dS - \oint_S T_{ij}(\mathbf{x}', \mathbf{x})u_j(\mathbf{x})dS + \\ &+ \int_S U_{ij}(\mathbf{x}', \mathbf{x})\gamma_{jk}n_k\theta dS - \int_V U_{ij}(\mathbf{X}', \mathbf{X})\gamma_{jk}\theta_{,k}dV \end{aligned} \tag{C.2}$$

Following the procedure explained in [38] the final thermoelastic integral displacement boundary equation is:

$$C_{ij}(\mathbf{x}')u_j(\mathbf{x}') + \fint_S T_{ij}(\mathbf{x}',\mathbf{x})u_j(\mathbf{x})dS = \int_S U_{ij}(\mathbf{x}',\mathbf{x})t_j(\mathbf{x})dS + \int_S Q_{\underline{ijk},\underline{t}}\gamma_{\underline{jk}}n_{\underline{t}}\theta d\hat{S} + \\ - \int_S Q_{\underline{ijk}}\gamma_{\underline{jk}}\theta_{,\underline{t}}n_{\underline{t}}d\hat{S} + \int_S U_{ij}(\mathbf{x}',\mathbf{x})\gamma_{jk}n_k\theta dS - \int_S U_{\underline{ij}}(\mathbf{x}',\mathbf{x})\gamma_{\underline{jk}}n_{\underline{k}}\theta d\hat{S} \tag{C.3}$$

where the function $Q_{\underline{ijk}}$ has been introduced such that:

$$Q_{\underline{ijk},\underline{tt}} = U_{\underline{ij},\underline{k}} \tag{C.4}$$

All the terms in Eq. (C.3) are now surface integrals: the ones relative to the mechanical quantities are expressed in the original domain, on the contrary the terms relative to the thermoelastic values are expressed in the mapped domain. Moreover the penultimate integral in Eq. (C.3) (also present in Eq. (C.2)) has been added in order to take into account the thermal effect ($\gamma_{jk}\theta$) on the stress tensor, and when the Cauchy's stress theorem is applied, $\gamma_{jk}\theta n_k$ has to be intended as a traction component (t_j). The last integral then is exactly equivalent to the penultimate but written in the mapped domain; when the Jacobian of the transformation is applied and the mapped quantities are expressed in the original domain, bearing in mind that $U_{ij} = U_{\underline{ij}}$ (as it will be shown later), the last two integrals neglect each other in the orthotropic case. Hence Eq. (C.3) can be rewritten as:

$$C_{ij}(\mathbf{x}')u_j(\mathbf{x}') = \int_S U_{ij}(\mathbf{x}',\mathbf{x})t_j(\mathbf{x})dS - \fint_S T_{ij}(\mathbf{x}',\mathbf{x})u_j(\mathbf{x})dS \\ \int_{\hat{S}} P_{\underline{i}}(\mathbf{x}',\mathbf{x})\theta(\mathbf{x})d\hat{S} - \int_S Q_{\underline{i}}(\mathbf{x}',\mathbf{x})q(\mathbf{x})dS \tag{C.5}$$

where the following manipulations have been done:

$$P_{\underline{i}} = Q_{\underline{ijj},\underline{t}}\gamma_{\underline{jj}}n_{\underline{t}} = (Q_{\underline{i11},\underline{1}}\gamma_{\underline{11}} + Q_{\underline{i22},\underline{1}}\gamma_{\underline{22}})n_{\underline{1}} + (Q_{\underline{i11},\underline{2}}\gamma_{\underline{11}} + Q_{\underline{i22},\underline{2}}\gamma_{\underline{22}})n_{\underline{2}} \tag{C.6}$$

$$\theta_{,\underline{t}}n_{\underline{t}}d\hat{S} = \theta_{,\underline{t}}n_{\underline{t}}JdS = q(\mathbf{x})dS \tag{C.7}$$

and

$$Q_{\underline{i}} = -Q_{\underline{ijj}}\gamma_{\underline{jj}}\frac{l}{\hat{l}}\frac{1}{\sqrt{k_{11}k_{22}}} = -(Q_{\underline{i11}}\gamma_{\underline{11}} + Q_{\underline{i22}}\gamma_{\underline{22}})\frac{l}{\hat{l}}\frac{1}{\sqrt{k_{11}k_{22}}} \tag{C.8}$$

The displacement and traction fundamental solution are then respectively given by:

$$U_{ij}(z_k^{'}, z_k) = 2Re[p_{j1}A_{i1}\log(z_1) + p_{j2}A_{i2}\log(z_2)] \tag{C.9}$$

$$T_{ij}(z_k^{'}, z_k) = 2Re\left[\frac{1}{z_1}q_{j1}(\mu_1 n_1 - n_2)A_{i1} + \frac{1}{z_2}q_{j2}(\mu_2 n_1 - n_2)A_{i2}\right] \tag{C.10}$$

where n_1 and n_2 are the component of the normal unit vector $\mathbf{n}$.

$\boldsymbol{\mu}$ can be expressed in matrix form for both domains as:

$$\boldsymbol{\mu} = \begin{bmatrix} 1 & 1 \\ \mu_1 & \mu_2 \end{bmatrix} \qquad \hat{\boldsymbol{\mu}} = \begin{bmatrix} \sqrt{\frac{k_{11}}{k_{22}}} & \sqrt{\frac{k_{11}}{k_{22}}} \\ \mu_1 & \mu_2 \end{bmatrix} \tag{C.11}$$

hence the following relationship applies:

$$\begin{cases} z_{\underline{1}} = \mu_{\underline{11}} x_{\underline{1}} + \mu_{\underline{21}} x_{\underline{2}} = \mu_{11} x_1 + \mu_{21} x_2 = z_1 \\ z_{\underline{2}} = \mu_{\underline{12}} x_{\underline{1}} + \mu_{\underline{22}} x_{\underline{2}} = \mu_{12} x_1 + \mu_{22} x_2 = z_2 \end{cases} \tag{C.12}$$

In virtue of Eq. (C.9) and (C.12) it is then clear why $U_{ij} = U_{\underline{ij}}$. Hence the functions in Eq. (C.6) and (C.8) take the form:

$$Q_{\underline{ijk}} = 2Re\left[\frac{p_{j1} A_{i1} \mu_{\underline{k1}} z_{\underline{1}} \log z_{\underline{1}}}{\mu_{\underline{11}}^2 + \mu_{\underline{21}}^2} + \frac{p_{j2} A_{i2} \mu_{\underline{k2}} z_{\underline{2}} \log z_{\underline{2}}}{\mu_{\underline{12}}^2 + \mu_{\underline{22}}^2}\right] \tag{C.13}$$

$$Q_{\underline{ijk},\underline{t}} = 2Re\left[\frac{p_{j1} A_{i1} \mu_{\underline{k1}}}{\mu_{\underline{11}}^2 + \mu_{\underline{21}}^2} \mu_{\underline{t1}} (\log z_{\underline{1}} + 1) + \frac{p_{j2} A_{i2} \mu_{\underline{k2}}}{\mu_{\underline{12}}^2 + \mu_{\underline{22}}^2} \mu_{\underline{t2}} (\log z_{\underline{2}} + 1)\right] \tag{C.14}$$

The above fundamental solutions can be expressed in real form for othotropic materials, as follows:

$$\mathbf{U}(\mathbf{x}', \mathbf{x}) = \begin{bmatrix} \frac{1}{b}(\sqrt{a_1} A_2^2 \log r_1 - \sqrt{a_2} A_1^2 \log r_2) & \frac{1}{b} A_1 A_2 (\theta_2 - \theta_1) \\ \frac{1}{b} A_1 A_2 (\theta_2 - \theta_1) & \frac{1}{b}\Big(\frac{A_2^2 \log r_2}{\sqrt{a_2}} - \frac{A_1^2 \log r_1}{\sqrt{a_1}}\Big) \end{bmatrix} \tag{C.15}$$

$$\mathbf{T}(\mathbf{x}', \mathbf{x}) = \begin{bmatrix} \frac{1}{b}\mathbf{x}\cdot\mathbf{n}\Big(\frac{A_1}{\sqrt{a_2} r_2^2} - \frac{A_2}{\sqrt{a_1} r_1^2}\Big) & \frac{1}{b}\Big(\frac{M_1 A_2}{r_1^2} - \frac{M_2 A_1}{r_2^2}\Big) \\ \frac{1}{b}\Big(\frac{M_1 A_1}{a_1 r_1^2} - \frac{M_2 A_2}{a_2 r_2^2}\Big) & \frac{1}{b}\mathbf{x}\cdot\mathbf{n}\Big(\frac{A_1}{\sqrt{a_1} r_1^2} - \frac{A_2}{\sqrt{a_2} r_2^2}\Big) \end{bmatrix} \tag{C.16}$$

$$\begin{bmatrix} Q_{\underline{111},1} \\ Q_{\underline{122},1} \\ Q_{\underline{211},1} \\ Q_{\underline{222},1} \end{bmatrix} = \begin{bmatrix} \frac{a_1^{3/2} A_2^2 k_{11}(1+\log r_1)}{b(a_1 k_{11} - k_{22})} - \frac{a_2^{3/2} A_1^2 k_{11}(1+\log r_2)}{b(a_2 k_{11} - k_{22})} \\ -\frac{A_1 A_2 \sqrt{a_1 k_{11} k_{22}}(1+\log r_1)}{b(a_1 k_{11} - k_{22})} + \frac{A_1 A_2 \sqrt{a_2 k_{11} k_{22}}(1+\log r_2)}{b(a_2 k_{11} - k_{22})} \\ -\frac{a_1 A_1 A_2 k_{11} \theta_1}{b(a_1 k_{11} - k_{22})} + \frac{a_2 A_1 A_2 k_{11} \theta_2}{b(a_2 k_{11} - k_{22})} \\ \frac{A_1^2 \sqrt{k_{11} k_{22}} \theta_1}{b(a_1 k_{11} - k_{22})} - \frac{A_2^2 \sqrt{k_{11} k_{22}} \theta_2}{b(a_2 k_{11} - k_{22})} \end{bmatrix} \tag{C.17}$$

$$\begin{bmatrix} Q_{\underline{111},2} \\ Q_{\underline{122},2} \\ Q_{\underline{211},2} \\ Q_{\underline{222},2} \end{bmatrix} = \begin{bmatrix} -\dfrac{a_1 A_2^2 \sqrt{k_{11}k_{22}}\theta_1}{b(a_1 k_{11} - k_{22})} + \dfrac{a_2 A_1^2 \sqrt{k_{11}k_{22}}\theta_2}{b(a_2 k_{11} - k_{22})} \\ \dfrac{A_1 A_2 k_{22}\theta_1}{b(a_1 k_{11} - k_{22})} - \dfrac{A_1 A_2 k_{22}\theta_2}{b(a_2 k_{11} - k_{22})} \\ -\dfrac{A_1 A_2 \sqrt{a_1 k_{11} k_{22}}(1 + \log r_1)}{b(a_1 k_{11} - k_{22})} + \dfrac{A_1 A_2 \sqrt{a_2 k_{11} k_{22}}(1 + \log r_2)}{b(a_2 k_{11} - k_{22})} \\ \dfrac{A_1^2 k_{22}(1 + \log r_1)}{\sqrt{a_1} b(a_1 k_{11} - k_{22})} - \dfrac{A_2^2 k_{22}(1 + \log r_2)}{\sqrt{a_2} b(a_2 k_{11} - k_{22})} \end{bmatrix} \tag{C.18}$$

$$\begin{bmatrix} Q_{\underline{111}} \\ Q_{\underline{122}} \\ Q_{\underline{211}} \\ Q_{\underline{222}} \end{bmatrix} = \begin{bmatrix} \dfrac{a_1 A_2^2 \sqrt{k_{11}k_{22}}(-x_2\theta_1 + \sqrt{a_1}x_1 \log r_1)}{b(a_1 k_{11} - k_{22})} - \dfrac{a_2 A_1^2 \sqrt{k_{11}k_{22}}(-x_2\theta_2 + \sqrt{a_2}x_1 \log r_2)}{b(a_2 k_{11} - k_{22})} \\ -\dfrac{A_1 A_2 k_{22}(-x_2\theta_1 + \sqrt{a_1}x_1 \log r_1)}{b(a_1 k_{11} - k_{22})} + \dfrac{A_1 A_2 k_{22}(-x_2\theta_2 + \sqrt{a_2}x_1 \log r_2)}{b(a_2 k_{11} - k_{22})} \\ -\dfrac{A_1 A_2 \sqrt{a_1 k_{11} k_{22}}(\sqrt{a_1}x_1\theta_1 + x_2 \log r_1)}{b(a_1 k_{11} - k_{22})} + \dfrac{A_1 A_2 \sqrt{a_1 k_{11} k_{22}}(\sqrt{a_2}x_1\theta_2 + x_2 \log r_2)}{b(a_2 k_{11} - k_{22})} \\ \dfrac{A_1^2 k_{22}(\sqrt{a_1}x_1\theta_1 + x_2 \log r_1)}{\sqrt{a_1} b(a_1 k_{11} - k_{22})} - \dfrac{A_2^2 k_{22}(\sqrt{a_2}x_1\theta_2 + x_2 \log r_2)}{\sqrt{a_2} b(a_2 k_{11} - k_{22})} \end{bmatrix} \tag{C.19}$$

According to Eq. (C.6) and (C.8), the functions involved in the thermoelastic fundamental solution $P_{\underline{i}}(\mathbf{x}', \mathbf{x})$ are shown in Eq. (C.17) and (C.18); Equation (C.19) shows the functions of the thermoelastic fundamental solution $Q_{\underline{i}}(\mathbf{x}', \mathbf{x})$.

It is now due to address an issue concerning the continuity of $\log(z)$ along the domain [37, 38]. The variable z can be explicitly expressed in function of a real and an imaginary component as:

$$z = \eta_1 + i\eta_2 \tag{C.20}$$

This is achieved with two consecutive coordinate transformations: a first mapping, which is equivalent to moving the origin of the coordinate system on the collocation point, is:

$$\begin{cases} \xi_1 = x_1 - x_1' \\ \xi_2 = x_2 - x_2' \end{cases} \tag{C.21}$$

and a second mapping in order to obtain the plane (η_1, η_2) is:

$$\begin{cases} \eta_1 &= \xi_1 + a\xi_2 = \xi_1 \\ \eta_2 &= b\xi_2 = \dfrac{\xi_2}{\sqrt{a_k}} \end{cases} \tag{C.22}$$

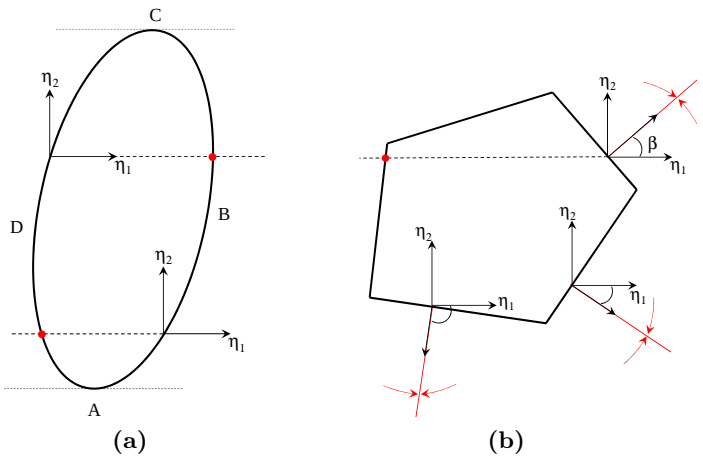


Figure C.9: (a) Simply connected domain and branch cut; (b) branch cut redefinition.

where $a = 0$ and $b = 1/\sqrt{a_k}$ for orthotropic materials ($\mu = a + ib$): the domain is not subject to any distortion and any point on the negative ξ_1 remains on the negative η_1. As it can be seen from the fundamental solutions in Eq. (C.15) and (C.17-C.19), the functions contain the term $\theta_k = Arg(z_k)$ since $\log(z)$ for a complex variable is defined as:

$$\log(z) = \log|z| + iArg(z) \tag{C.23}$$

When the principal value of $Arg(z)$ is assumed:

$$-\pi < Arg(z) \leq \pi \tag{C.24}$$

the function $Arg(z) = Arg(\eta_1 + i\eta_2)$ has a branch cut along the negative η_1 axis, where it is not defined. In order to circumvent this problem simply-connected convex domains have been considered in this work as the one shown in Figure C.9(a).

Depending on the position of the collocation point, one of the semi-axis always cuts the domain boundary and collocation on the portion ABC would generate a discontinuity in the function $\log(z)$ along the negative η_1.

It is for this reason that in this work, in order to overcome the problem of the continuity of the function $Arg(z)$ along the domain, a rule that is generic and easy to automatically implement has been applied to the case of simply-connected domains. Calling β the angle between the local outward normal direction and the positive η_1 semi-axis, where the domain of β is defined as:

$$-\pi < \beta \leq \pi \tag{C.25}$$

the domain of the function $Arg(z)$ can be redefined locally as:

$$\beta < Arg(z) \leq \beta + 2\pi \tag{C.26}$$

In other words in this way the branch cut is always moved along the local outward normal direction, as shown in Figure C.9(b), and hence away from the domain.

This re-definition also applies to non-convex domains as long as the local normal does not cut the domain in any point, which happens when the concavity is not too pronounced or sharp.

On the other hand if multiply-connected domains are considered or collocation point is chosen in any internal point, the redefinition of the argument's domain would never solve the discontinuity problem and the addition of a series of line integrals along the negative η_1 is necessary, as explained in [38, 42]. In the present work however the additional line integrals have not been considered and some assumptions have been done to justify this decision. The collocation on internal points or elements concerns respectively the stress or traction equation in the present formulation; after the evaluation of the fundamental solutions' derivatives, only the components of $Q_{\underline{ij}}$ contain $Arg(z)$, i.e. the term multiplying the flux. Hence two possible assumptions are proposed here:

1. In absence of (internal) heat source, the net flux across the outer domain boundaries is zero, so if the top, bottom, right and left edges of a rectangular domain are considered, it is possible to write the following relationships:

$$\begin{cases} q^{top} = -q^{bottom} \\ q^{right} = -q^{left} \end{cases} \tag{C.27}$$

   Hence assuming periodic boundary conditions, the stress or traction equation can be expressed in function of the fluxes of half of the outer domain (e.g. bottom and right edges): the integrations of the fundamental solutions relative to the flux variable need to be changed from each grain's domain to the external domain of the aggregate. In this way the integration along the remaining portion of the domain would not be necessary and consequently the discontinuity of $Arg(z)$ would not be a problem. The results obtained with this method have been compared with other numerical and analytical results for single domain problem, showing good agreement.
2. When microstructures are considered, the length scale under exam is 10^{-6} to 10^{-3} m, i.e. the mesoscale of the material. It is then plausible to assume that the thermal gradients in the whole structure are such that the one within the single polycrystalline aggregate (RVE for example) is not big and hence neglectable, resulting in a zero-flux condition for the single microstructure. In a multi-scale framework this assumption is equivalent to consider a macroscopic thermal gradient but with a discrete temperature profile, which is constant in each microstructure.

For the sake of simplicity the second assumption has been adopted in the polycrystalline simulations shown in the current work; the results do not change significantly compared to the expected ones with small fluxes, and the formulation for the present investigation becomes faster and easier to implement. Nevertheless the code developed is complete for cases where internal collocation is not required and ready to be further extended, but the improvement of the result is not worth the derived complexity of the formulation required for these applications, at this stage.

D. Local fields

Since each grain has an independent orthotropic elastic behaviour with generic planar orientation, the contribution of each tile to the whole structure might be fully anisotropic: the fourth order compliance (or stiffness) tensor in the material reference system, once expressed in the global reference system, is fully populated; thus in order to avoid the rotation of the fourth order compliance tensor and to be able to use the real form fundamental solutions written above, each grain coordinate expressed by $\mathbf{x}_{S^H} \in S^H : \mathbf{x}_{S^H} \subset \mathbb{R}^2$ is rotated to the material coordinates $\tilde{\mathbf{x}}_{\tilde{S}^H} \in \tilde{S}^H : \tilde{\mathbf{x}}_{\tilde{S}^H} \subset \mathbb{R}^2$. Thus all the prescribed boundary conditions are enforced in the local coordinate system of each element:

$$\begin{cases} \tilde{\mathbf{t}}^p = \mathbf{R}\ \mathbf{t}^p \\ \tilde{\mathbf{u}}^p = \mathbf{R}\ \mathbf{u}^p \end{cases} \tag{D.1}$$

where $\mathbf{t}^p$ and $\mathbf{u}^p$ are the prescribed tractions and displacements and $\mathbf{R}$ is the transformation matrix to rotate from global coordinate to normal and tangential local coordinate, where n_x and n_y are the components of the normal unit vector on the boundary S^H:

$$\mathbf{R} = \begin{bmatrix} -n_y & n_x \\ n_x & n_y \end{bmatrix} \tag{D.2}$$

Each grain is then rigidly rotated by the angle θ:

$$\tilde{\mathbf{x}}_{\tilde{S}^H} = \mathbf{R}_\theta\ \mathbf{x}_{S^H} \tag{D.3}$$

where

$$\mathbf{R}_\theta = \begin{bmatrix} \cos\theta & \sin\theta \\ -\sin\theta & \cos\theta \end{bmatrix} \tag{D.4}$$

Finally the fundamental solutions (originally expressed in material coordinates) need to be multiplied by a rotation matrix too, in order for them to correspond to the respective field in the local coordinate system of the interfaces t-n:

$$\begin{cases} \tilde{\mathbf{T}} = \mathbf{T}\ \tilde{\mathbf{R}} \\ \tilde{\mathbf{U}} = \mathbf{U}\ \tilde{\mathbf{R}} \end{cases} \tag{D.5}$$

$$\tilde{\mathbf{R}} = \begin{bmatrix} -\tilde{n}_y & \tilde{n}_x \\ \tilde{n}_x & \tilde{n}_y \end{bmatrix} \tag{D.6}$$

where $\tilde{n}_x$ and $\tilde{n}_y$ are the components of the normal unit vector on the boundary $\tilde{S}^H$.

References

[1] G. Geraci, M. Aliabadi, Micromechanical boundary element modelling of transgranular and intergranular cohesive cracking in polycrystalline materials, Engineering Fracture Mechanics 176 (2017) 351 – 374.

[2] I. Benedetti, M. H. Aliabadi, A three-dimensional cohesive-frictional grain-boundary micromechanical model for intergranular degradation and failure in polycrystalline materials, Computer Methods in Applied Mechanics and Engineering (2013) 36–62.

[3] J. Blendell, R. L. Coble, Measurement of stress due to thermal expansion anisotropy in al2o3, Journal of the American Ceramic Society 65 (3) (1982) 174–178.

[4] R. W. Rice, S. W. Freiman, P. F. Becher, Grain-size dependence of fracture energy in ceramics: i, experiment, Journal of the American ceramic society 64 (6) (1981) 345–350.

[5] R. W. Rice, S. W. Freiman, Grain-size dependence of fracture energy in ceramics: ii, a model for noncubic materials, Journal of the American Ceramic Society 64 (6) (1981) 350–354.

[6] R. W. Rice, R. C. Pohanka, Grain-size dependence of spontaneous cracking in ceramics, Journal of the American Ceramic Society 62 (11-12) (1979) 559–563.

[7] S. G. Yousef, J. Rödel, E. Fuller, A. Zimmermann, B. El-Dasher, Microcrack evolution in alumina ceramics: experiment and simulation, Journal of the American Ceramic Society 88 (10) (2005) 2809–2816.

[8] N. Sridhar, W. Yang, D. J. Srolovitz, E. R. Fuller, Microstructural mechanics model of anisotropic-thermal-expansion-induced microcracking, Journal of the American Ceramic Society 77 (5) (1994) 1123–1138.

[9] G. T. Camacho, M. Ortiz, Computational modelling of impact damage in brittle materials, International Journal of solids and structures 33 (20) (1996) 2899–2938.

[10] V. Tvergaard, Effect of fibre debonding in a whisker-reinforced metal, Materials science and engineering: A 125 (2) (1990) 203–213.

[11] X. P. Xu, A. Needleman, Numerical simulations of dynamic crack growth along an interface, International Journal of Fracture (1995-1996) 289–324.

[12] K. Park, G. H. Paulino, Cohesive zone models: a critical review of traction-separation relationships across fracture surfaces, Applied Mechanics Reviews 64 (6) (2011) 060802.

[13] N. Sukumar, D. J. Srolovitz, T. J. Baker, J. H. Prévost, Brittle fracture in polycrystalline microstructures with the extended finite element method, International Journal for Numerical Methods in Engineering 56 (14) (2003) 2015–2037.

[14] J. Qian, S. Li, Application of multiscale cohesive zone model to simulate fracture in polycrystalline solids, Journal of Engineering Materials and Technology 133 (1) (2011) 011010.

[15] L. Lin, X. Wang, X. Zeng, The role of cohesive zone properties on intergranular to transgranular fracture transition in polycrystalline solids, International Journal of Damage Mechanics (2015) 1056789515618732.

[16] H. D. Espinosa, P. D. Zavattieri, A grain level model for the study of failure initiation and evolution in polycrystalline brittle materials. part i: Theory and numerical implementation, Mechanics of Materials 35 (3) (2003) 333–364.

[17] H. D. Espinosa, P. D. Zavattieri, A grain level model for the study of failure initiation and evolution in polycrystalline brittle materials. part ii: numerical examples, Mechanics of Materials 35 (3) (2003) 365–394.

[18] S. Rangaraj, K. Kokini, A study of thermal fracture in functionally graded thermal barrier coatings using a cohesive zone model, Journal of engineering materials and technology 126 (1) (2004) 103–115.

[19] K. Willam, I. Rhee, B. Shing, Interface damage model for thermomechanical degradation of heterogeneous materials, Computer Methods in Applied Mechanics and Engineering 193 (30) (2004) 3327–3350.

[20] A. Sapora, M. Paggi, A coupled cohesive zone model for transient analysis of thermoelastic interface debonding, Computational Mechanics 53 (4) (2014) 845–857.

[21] T. Wu, P. Wriggers, Multiscale diffusion–thermal–mechanical cohesive zone model for concrete, Computational Mechanics 55 (5) (2015) 999–1016.

[22] I. Özdemir, W. Brekelmans, M. Geers, A thermo-mechanical cohesive zone model, Computational Mechanics 46 (5) (2010) 735–745.

[23] M. H. Aliabadi, Boundary element formulations in fracture mechanics, Applied Mechanics Reviews 50 (2) (1997) 83–96.

[24] G. Sfantos, M. Aliabadi, A boundary cohesive grain element formulation for modelling intergranular microfracture in polycrystalline brittle materials, International journal for numerical methods in engineering 69 (8) (2007) 1590–1626.

[25] I. Benedetti, V. Gulizzi, A. Milazzo, Grain-boundary modelling of hydrogen assisted intergranular stress corrosion cracking, Mechanics of Materials 117 (2018) 137 – 151.

[26] A. Portela, M. H. Aliabadi, D. P. Rooke, The dual boundary element method: effective implementation for crack problems, International Journal for Numerical Methods in Engineering 33 (6) (1992) 1269–1287.

[27] A. Portela, M. H. Aliabadi, D. P. Rooke, Dual boundary element incremental analysis of crack propagation, Computers & Structures 46 (2) (1993) 237–247.

[28] P. Sollero, M. H. Aliabadi, Anisotropic analysis of cracks in composite laminates using the dual boundary element method, Composite structures 31 (3) (1995) 229–233.

[29] M. Aliabadi, P. Sollero, Crack growth analysis in homogeneous orthotropic laminates, Composites science and technology 58 (10) (1998) 1697–1703.

[30] N. Prasad, M. Aliabadi, D. Rooke, The dual boundary element method for thermoelastic crack problems, International Journal of Fracture 66 (3) (1994) 255–272.

[31] N. Prasad, M. Aliabadi, D. Rooke, The dual boundary element method for transient thermoelastic crack problems, International journal of solids and structures 33 (19) (1996) 2695–2718.

[32] Z. Li, R. Bradt, Thermal expansion of the hexagonal (6h) polytype of silicon carbide, Journal of the American Ceramic Society 69 (12) (1986) 863–866.

[33] Z. Li, R. Bradt, Thermal expansion and thermal expansion anisotropy of sic polytypes, Journal of the American Ceramic Society 70 (7) (1987) 445–448.

[34] L. Onsager, Reciprocal relations in irreversible processes. i., Physical review 37 (4) (1931) 405.

[35] L. Onsager, Reciprocal relations in irreversible processes. ii., Physical review 38 (12) (1931) 2265.

[36] M. H. Aliabadi, The Boundary Element Method, Application in Solid and Structures, Wiley, London, 2002.

[37] Y. Shiah, C. Tan, Bem treatment of two-dimensional anisotropic field problems by direct domain mapping, Engineering Analysis with boundary elements 20 (4) (1997) 347–351.

[38] Y. Shiah, C. Tan, Exact boundary integral transformation of the thermoelastic domain integral in bem for general 2d anisotropic elasticity, Computational Mechanics 23 (1) (1999) 87–96.

[39] L. C. Wrobel, The boundary element method, applications in thermo-fluids and acoustics, Vol. 1, John Wiley & Sons, 2002.

[40] S. Nemat-Nasser, M. Hori, Micromechanics: overall properties of heterogeneous materials, Vol. 37, Elsevier, 2013.

[41] G. Sfantos, M. Aliabadi, Multi-scale boundary element modelling of material degradation and fracture, Computer Methods in Applied Mechanics and Engineering 196 (7) (2007) 1310–1329.

[42] J. Zhang, C. Tan, F. Afagh, A general exact transformation of body-force volume integral in bem for 2d anisotropic elasticity, Computational mechanics 19 (2) (1996) 1–10.